JGP Journal of General Physiology

ARTICLE

Resting and stimulated mouse rod photoreceptors show distinct patterns of vesicle release at ribbon synapses

Cassandra L. Hays[1,3], Asia L. Sladek[2], and Wallace B. Thoreson[2,3]

The vertebrate visual system can detect and transmit signals from single photons. To understand how single-photon responses are transmitted, we characterized voltage-dependent properties of glutamate release in mouse rods. We measured presynaptic glutamate transporter anion current and found that rates of synaptic vesicle release increased with voltage-dependent Ca^{2+} current. Ca^{2+} influx and release rate also rose with temperature, attaining a rate of ∼11 vesicles/s/ribbon at −40 mV (35°C). By contrast, spontaneous release events at hyperpolarized potentials (−60 to −70 mV) were univesicular and occurred at random intervals. However, when rods were voltage clamped at −40 mV for many seconds to simulate maintained darkness, release occurred in coordinated bursts of 17 ± 7 quanta (mean ± SD; *n* = 22). Like fast release evoked by brief depolarizing stimuli, these bursts involved vesicles in the readily releasable pool of vesicles and were triggered by the opening of nearby ribbon-associated Ca^{2+} channels. Spontaneous release rates were elevated and bursts were absent after genetic elimination of the Ca^{2+} sensor synaptotagmin 1 (Syt1). This study shows that at the resting potential in darkness, rods release glutamate-filled vesicles from a pool at the base of synaptic ribbons at low rates but in Syt1-dependent bursts. The absence of bursting in cones suggests that this behavior may have a role in transmitting scotopic responses.

Introduction

The exquisite visual sensitivity of vertebrates originates with the ability of rod photoreceptor cells in the retina to detect single photons. In darkness, rods have a resting membrane potential near −40 mV, sufficiently depolarized to activate Ca_V α subunit 1.4 ($Ca_V1.4$) L-type Ca^{2+} channels that control synaptic glutamate release (Pangrsic et al., 2018). Unlike most voltage-gated Ca^{2+} channels, $Ca_V1.4$ channels show minimal voltage- and Ca^{2+}-dependent inactivation, allowing continued Ca^{2+} influx into rod terminals during maintained darkness (Baumann et al., 2004; Koschak et al., 2003; McRory et al., 2004; Waldner et al., 2018). The maintained release of glutamate from rods is also facilitated by the presence of a platelike presynaptic structure known as the synaptic ribbon (Heidelberger et al., 2005; Schmitz, 2009). Ribbons help to capture and tether vesicles along their planar surfaces, delivering them to release sites at the base (Snellman et al., 2011; Vaithianathan et al., 2016; Wen et al., 2018). In amphibian retina, it has been shown that synaptic release from rods varies linearly with Ca^{2+} influx, translating light-evoked voltage responses into changes in the rate of glutamate release that act on second-order neurons (Rieke and Schwartz, 1996; Thoreson et al., 2004). Release from mammalian rods is regulated by the exocytotic Ca^{2+} sensor molecule synaptotagmin 1 (Syt1), although there is also evidence for a second sensor (Grassmeyer et al., 2019). Syt1 is absent from amphibian rods (Heidelberger et al., 2003), suggesting that properties of release may differ among vertebrate genera.

Absorption of a single photon by rods produces voltage changes of only a few millivolts (Cangiano et al., 2012; Schneeweis and Schnapf, 1995). Second-order rod bipolar cells are faced with the challenge of distinguishing genuine light-evoked changes in release rate produced by these small voltage changes from random intervals in release. One strategy for overcoming this problem is to maintain a high rate of glutamate release so that small changes in membrane voltage cause a large enough reduction in release to be distinguished from basal rates (Rao-Mirotznik et al., 1998; Rao et al., 1994; van Rossum and Smith, 1998). Modeling studies suggest that success with this approach requires release rates of ≥100 vesicles/s/ribbon, but imaging studies with the activity-dependent dye FM1-43, suggest that release rates in gecko and salamander rods are only 2.5 and 18 vesicles/s/ribbon, respectively (Sheng et al.,

[1]Cellular and Integrative Physiology, College of Medicine, University of Nebraska Medical Center, Omaha, NE; [2]Pharmacology and Experimental Neuroscience, College of Medicine, University of Nebraska Medical Center, Omaha, NE; [3]Truhlsen Eye Institute and Department of Ophthalmology and Visual Sciences, College of Medicine, University of Nebraska Medical Center, Omaha, NE.

Correspondence to Wallace B. Thoreson: wbthores@unmc.edu.

2007). Release rates have not been measured in mammalian rods.

In this study, we measured voltage-dependent changes in rates of release from individual mouse rods that each possess a single ribbon synapse. Measuring release events postsynaptically is complicated by the convergence of many rods onto a single bipolar cell (Behrens et al., 2016; Tsukamoto and Omi, 2013). Furthermore, individual quantal release events cannot be observed in ON bipolar cell recordings due to the slow kinetics of the mGluR6 transduction cascade (Berntson et al., 2004; Berntson and Taylor, 2003). To detect individual release events, we took advantage of the fact that the presynaptic glutamate transporters in rod terminals (largely excitatory amino-acid transporter 5 [EAAT5]) are linked to an uncoupled anion conductance so that an anion channel is opened as glutamate is retrieved (Arriza et al., 1997; Schneider et al., 2014). The anion current is linearly proportional to glutamate in the cleft (Otis and Jahr, 1998) and can thus serve as a presynaptic measure of release (Hasegawa et al., 2006). Our measurements of glutamate transporter anion current ($I_{A(glu)}$) showed that release rates increased linearly with Ca^{2+} influx but rose only to ∼11 vesicles/s/ribbon at −40 mV (35°C). When rods were voltage clamped at −70 mV, we saw spontaneous release of single vesicles at random intervals, but release at −40 mV involved bursts of ∼17 vesicles apiece spaced at more regular intervals. These bursts required coordination by Syt1. Our experiments indicate that bursts at −40 mV involve vesicles in the readily releasable pool at the base of the ribbon and are triggered by opening of nearby Ca^{2+} channels. Lowering distant Ca^{2+} levels lengthened interevent intervals between bursts, perhaps by influencing ribbon replenishment rates. The presence of these bursts in rods but not cones and their appearance near the resting membrane potential in darkness suggest they may play a role in transmitting rod responses under scotopic conditions.

Materials and methods

Animals

Control and mutant mice were kept on 12-h dark/light cycles. Animal handling and experimental protocols were approved by the University of Nebraska Medical Center Institutional Animal Care and Use Committee. Mice of both sexes aged 4–12 wk were euthanized in accordance with the American Veterinary Medical Association Guidelines for the Euthanasia of Animals by CO_2 asphyxiation followed by cervical dislocation.

$Rod^{Syt1cko}$ mutants in which Syt1 was selectively eliminated from rods were bred by crossing *Rho-iCre* mice (RRID: ISMR_JAX:015850) with $Syt1^{flox}$ mice (Syt1: MGI:99667) in which *LoxP* sites flank exon 6 of *Syt1* (Quadros et al., 2017). $Syt1^{flox}$ mice were originally created on a C57/BL6N background. Genetic screening showed that mice used for these experiments were 40% C57/BL6J.

Electrophysiology

Rod cells were visualized in a flat mount preparation on an upright fixed-stage microscope (Nikon E600FN) using a 60×, 1.0 NA water immersion objective. Rods were identified visually and targeted with positive pressure using recording electrodes mounted on Huxley-Wall micromanipulators (Sutter Instruments). Rod recordings were performed in whole-cell voltage clamp mode using a Multiclamp 700A amplifier (Axon Instruments/Molecular Devices), and signals were digitized with DigiData 1550 (Axon Instruments/Molecular Devices). Data acquisition and analysis were performed using pClamp 10 software (Molecular Devices).

Flat mount preparations were continuously superfused with room temperature Ames solution (US Biological) bubbled with 95% O_2/5% CO_2 at ∼1 ml/min. In some experiments, we used an inline heater to heat the superfusate to 35°C. We calculated the Q_{10} (temperature coefficient describing the change produced by a 10°C increase in temperature) for $I_{A(glu)}$ frequency and Ca^{2+} currents (I_{Ca}) amplitude using the following equation:

$$Q_{10} = \left(\frac{F_H}{F_L}\right)^{10/\Delta T},$$

where F_H and F_L are the features of interest at high and low temperatures, respectively, and ΔT is the absolute value of the difference in temperature in degrees centigrade.

Intracellular pipette solutions for $I_{A(glu)}$ measurements contained thiocyanate (SCN^-) to enhance anion currents and consisted of (in mM): 120 KSCN, 10 TEA-Cl, 10 HEPES, 1 $CaCl_2$, 1 $MgCl_2$, 0.5 Na-GTP, 5 Mg-ATP, and 5 phosphocreatine (pH 7.3). Intracellular Ca^{2+} was buffered with 5 mM EGTA unless otherwise noted. For I_{Ca} measurements, Cs-gluconate replaced KSCN, and Ca^{2+} buffering was reduced to 2 mM EGTA. Passive membrane properties measured with KSCN pipette solution showed an average membrane capacitance of 3.2 ± 0.2 pF and membrane resistance of 2.3 ± 0.04 GΩ (mean ± SD; n = 20). Voltages were not corrected for liquid junction potentials unless specifically noted (Cs-gluconate pipette solution, 12.3 mV; KSCN pipette solution, 3.9 mV).

$I_{A(glu)}$ events were identified and measured for frequency, kinetics, and charge transfer with the event finder function in pClamp directed by a template averaged from ∼10 events. Data were acquired from one to three rods per animal. Statistical analysis was performed using GraphPad Prism 7 and 8 software, and data are reported as mean ± SD unless otherwise noted.

Online supplemental material

Fig. S1 shows data illustrating that CICR and feedback from horizontal cells are not required for bursting behavior in rods. Fig. S2 shows illustrations of large Ca^{2+}-activated Cl^- currents that were occasionally activated during depolarizing stimulation.

Results

Voltage-dependent release properties

Presynaptic recordings of $I_{A(glu)}$ in voltage-clamped rods can provide a reliable presynaptic measure of glutamate release, reflecting the timing and magnitude of exocytotic events (Grassmeyer et al., 2019; Hasegawa et al., 2006; Szmajda and Devries, 2011). In several experimental systems, including rods

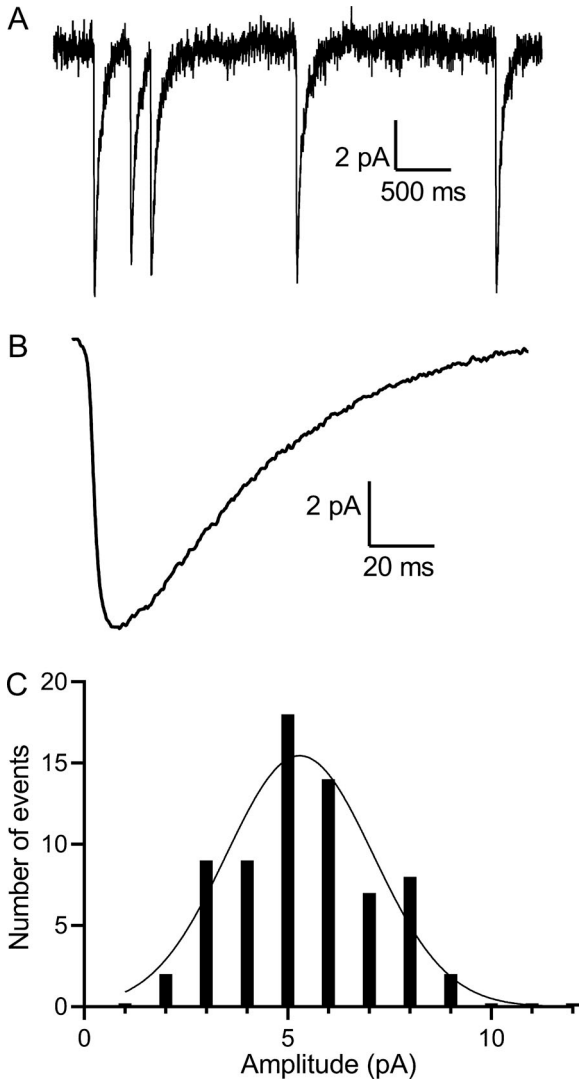

Figure 1. **Spontaneous $I_{A(glu)}$ release events observed in rods held at −70 mV. (A)** Example trace from a rod voltage clamped at −70 mV showing spontaneous unitary $I_{A(glu)}$ release events. **(B)** Waveform averaged from 45 unitary $I_{A(glu)}$ events in a single rod. **(C)** Amplitude frequency distributions of $I_{A(glu)}$ events measured in a rod at −70 mV were well described by a single Gaussian, suggesting they arose from single-vesicle fusion events (5.6 ± 1.7 pA, mean ± SD; *n* = 12; 187 events).

and cones, the anionic charge transfer has been shown to be proportional to glutamate concentrations in the cleft and likewise proportional to excitatory postsynaptic currents (Hays et al., 2020; Koch et al., 2007; Otis and Jahr, 1998; Szmajda and Devries, 2011). To measure glutamate release presynaptically, we obtained whole-cell recordings from mouse rods using the permeant SCN^- as the principal anion in the patch pipette solution to enhance $I_{A(glu)}$. When rods were voltage clamped at −70 mV, we observed occasional spontaneous presynaptic currents averaging 5.6 ± 1.7 pA (*n* = 187 events in 12 rods, 8 animals; Fig. 1). As illustrated by the average event shown in Fig. 1, these events exhibited a waveform typical of quantal postsynaptic currents but with slow kinetics, showing a 10–90% rise time of 9.3 ± 1.3 ms and decay time constant of 39.9 ± 9.9 ms (*n* > 10 events in each of 12 rods). The rising phase of $I_{A(glu)}$ integrates rising glutamate levels in the synaptic cleft (Hays et al., 2020; Szmajda and Devries, 2011). The slow rate of decline reflects the slow cycle time of glutamate transport (Gameiro et al., 2011; Palmer et al., 2003). Event amplitude histograms assumed the shape of a single Gaussian function, suggesting that the distribution consists primarily of single-vesicle fusion events (Fig. 1 C).

$I_{A(glu)}$ release events originated from the voltage-clamped rod. We predicted that if glutamate released from neighboring rods and cones could reach transporters in the voltage-clamped rod, then depolarizing the surrounding photoreceptors by bath application of a solution containing 30 mM K^+ should increase the number of small events. However, application of 30 mM K^+ did not increase event frequency at −70 mV compared with control extracellular solution in the same cells (0.87 ± 0.5 versus 0.62 ± 0.1 quanta/s; P = 0.28; *n* = 3 rods, 1 animal), nor did it change the 10–90% rise time (11.3 ± 8.0 ms versus 10.5 ± 6.5 ms; P = 0.36; *n* = 3 rods) or magnitude of unitary events (4.16 ± 1.82 versus 5.40 ± 2.00 pA; P = 0.47; *n* = 3 rods). Likewise, hyperpolarizing surrounding photoreceptors by applying a bright white light did not decrease baseline noise that would have been generated from extrasynaptic glutamate (mean ± SD = 0.50 ± 0.03 pA versus 0.52 ± 0.18 pA; P = 0.79; *n* = 5 rods, unpaired *t* test).

As illustrated in Fig. 2 A, the character of release changed dramatically as the membrane potential approached −40 mV. All of the spontaneous release events observed when rods were held at −70 mV were uniquantal, showing a unimodal amplitude distribution (Fig. 1 C). However, at −40 mV, rods consistently switched to a more regular bursting behavior with release of many vesicles in each burst (Fig. 2 A, arrowheads). Consistent with earlier findings from mouse rods (Grassmeyer et al., 2019), both bursts and uniquantal $I_{A(glu)}$ events in mouse rods were blocked by bath application of the glutamate transport inhibitor threo-β-benzyloxyaspartate (TBOA; 100 µM), confirming that they reflect glutamate transporter activity (*n* = 5 rods, 2 animals; Fig. 2 B). Bursts were not a consequence of using KSCN in the patch pipette to enhance $I_{A(glu)}$, since we observed similar, albeit smaller, bursts using a CsCl-based pipette solution (*n* = 4 rods, 3 animals).

To estimate the number of vesicles released during each bursting episode, the charge transfer of each burst was divided by the average charge transfer of occasional unitary events measured at the same potential in the same cell. Because of the high density of EAAT5 glutamate transporters in rods, glutamate reuptake increases even after saturation of postsynaptic mGluR6 receptors, indicating that transporters do not become saturated during release from rods (Hasegawa et al., 2006). We assumed that individual $I_{A(glu)}$ events summed linearly and thus used charge transfer measurements to count the number of release events during 30-s steps at various holding potentials. The number of quanta in 10-s intervals shown in Fig. 2 is indicated at the right for each trace. In this example, there were 5 unitary release events at −70 mV during the 10-s period and 64 events at −40 mV, the latter occurring in periodic, coordinated bursts of release.

The overall rate of vesicle release measured in this way increased gradually with membrane depolarization (Fig. 2). The

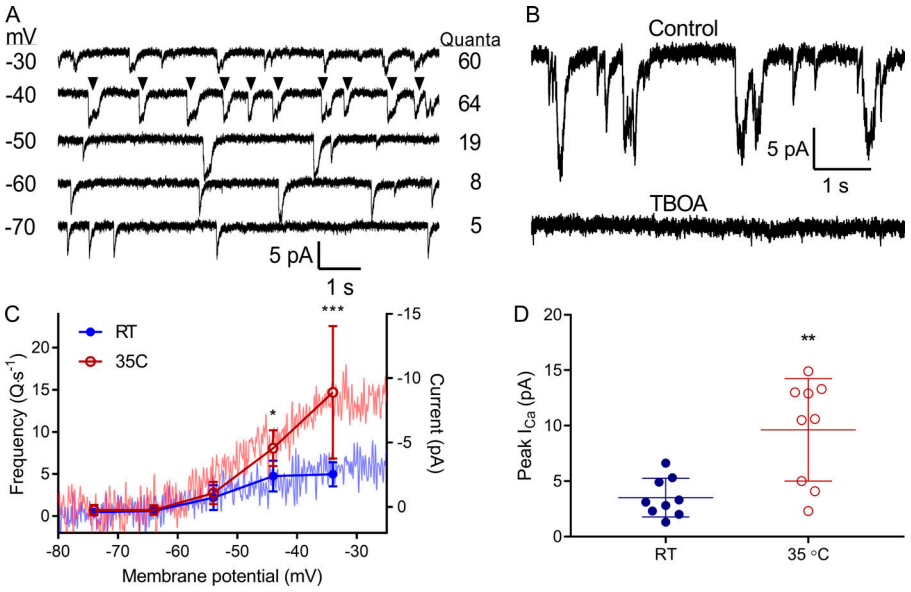

Figure 2. **Voltage and temperature dependence of vesicle release rates in rods. (A)** $I_{A(glu)}$ vesicle release events in rods increased in frequency with depolarization. As the holding potential approached −40 mV, release events were organized in bursts of 10–20 vesicles (black arrowheads) rather than unitary events that predominated in rods held at −70 mV. The number of quanta in a burst was calculated by measuring the burst charge transfer and then dividing it by the charge transfer of a unitary event measured in the same cell at that voltage. The number of quanta released during each trace is denoted at the right of each trace. **(B)** Bath application of the glutamate transport inhibitor TBOA (0.3 mM) abolished both bursts and uniquantal $I_{A(glu)}$ events in a rod held at −30 mV. **(C)** Rates of release (circles) increased in parallel with I_{Ca} (traces) at room temperature and 35°C. Open red circles show release rates at 35°C (n = 5 rods, 4 animals), and filled blue circles show rates at room temperature (n = 9 rods, 3 animals). Blue and red traces show I_{Ca} averaged from nine rods measured at room temperature and 35°C, respectively. Both voltage and temperature affect release rate (P < 0.001, two-way ANOVA). Release rates at −44 and −34 mV were increased significantly by temperature (P = 0.03 and P = 0.0002, respectively, two-way ANOVA, Tukey's multiple comparisons test). **(D)** The peak amplitude of I_{Ca} increased significantly from room temperature (filled blue circles) to 35°C (open red circles; P = 0.004, paired t test; n = 9 rods, 3 animals). *, P < 0.05; **, P < 0.01; ***, P < 0.0001; t tests. Error bars show mean ± SD. Q, quanta.

increase in release rate tracked voltage-dependent increases in I_{Ca} (Fig. 2 C), similar to the linear relationship between I_{Ca} and release observed in amphibian rods (Thoreson et al., 2004). I_{Ca} was measured in mouse rods using voltage ramps and Cs-gluconate rather than KSCN as the principal ions in the pipette solution. Fig. 2 C plots the voltage-dependent changes in release on the same graph as the voltage dependence of I_{Ca} after correcting for the different liquid junction potentials. Increasing temperature to 35°C from room temperature (20°C) nearly doubled peak Ca^{2+} influx and caused a proportional increase in release rate (Fig. 2 D). The Q_{10} values for I_{Ca} and release rate at −30 mV were nearly identical (2.09 ± 0.78 for I_{Ca}, n = 9 rods, 3 animals; 2.10 ± 1.22 for release, n = 6 rods, 4 animals). Temperature can affect gating properties of voltage-gated channels, but as with $Ca_V1.4$ currents in transfected HEK cells, where the window current was unchanged (Peloquin et al., 2008), the midpoint activation voltage for I_{Ca} in our experiments was not shifted by temperature (Q_{10} = 1.03 ± 0.02).

Interburst intervals were shortened at higher temperatures, largely accounting for the increase in release rate at depolarized potentials (interburst interval room temperature = 2,756 ± 596 ms, n = 14; 35°C = 1,130 ± 665 ms, n = 5 rods, 5 animals; P < 0.001, unpaired t test). The number of quanta in each burst at −40 mV (−43.9 mV after correcting for liquid junction potential) did not increase significantly (17 ± 7 at room temperature, n = 22 rods, 15 animals, versus 11 ± 6 at 35°C, n = 5 rods, 5 animals; P = 0.5, unpaired t test). Bursts showed faster kinetics with a narrower half-width at higher temperatures (room temperature, 216 ± 69 ms, n = 22; 35°C, 125 ± 33 ms, n = 5; P = 0.03, unpaired t test, n = 5).

Unitary events were occasionally interspersed between bursts. The example in Fig. 3 A comes from a rod that showed numerous small unitary events with a mean amplitude of 4 pA interspersed among larger bursts that averaged 12 pA in amplitude when the rod was held at −40 mV. The amplitude of unitary fusion events diminished with membrane depolarization because of the diminished outward driving force for SCN^- at more depolarized potentials (Arriza et al., 1997; Torres-Salazar and Fahlke, 2007; n = 6 cells, 6 animals; open triangles in Fig. 3 B). However, as illustrated by the filled circles in Fig. 3 B, when we plotted the mean amplitude of all events—both bursts and unitary events—from this cell together, average $I_{A(glu)}$ amplitude initially increased as a function of membrane voltage and then decreased. This initial increase occurred despite a decline in anion driving force and likely resulted from an increase in the number of multiquantal bursts at more depolarized potentials. The average amplitude then diminished with a further decline in anion driving force with further depolarization above −40 mV.

Bursts showed inflection points during the initial inward current, suggesting they arose from sequential fusion of individual vesicles (e.g., Fig. 2, A and B). The examples in Fig. 3, C and D, show increases in $I_{A(glu)}$ punctuated by inflections at intervals that were roughly the same amplitude as the corresponding single-vesicle events. This suggests that the rising phase consisted of rapid sequential fusion of three vesicles. One could also see individual peaks during the plateau phase of bursts, suggesting that additional fusion events contributed to maintaining the bursts. Event half-widths in room temperature varied widely (60–709 ms) but averaged 216 ± 69 ms (n = 22 rods, 15 animals).

Bursts were both longer in duration and larger in amplitude than individual events. Fig. 3 E shows an amplitude histogram for events measured at a holding potential of −40 mV from the rod shown in Fig. 3 A. This rod was chosen for this illustration because it showed an abundance of unitary events at −40 mV. When fit with a multiple Gaussian, the amplitude histogram

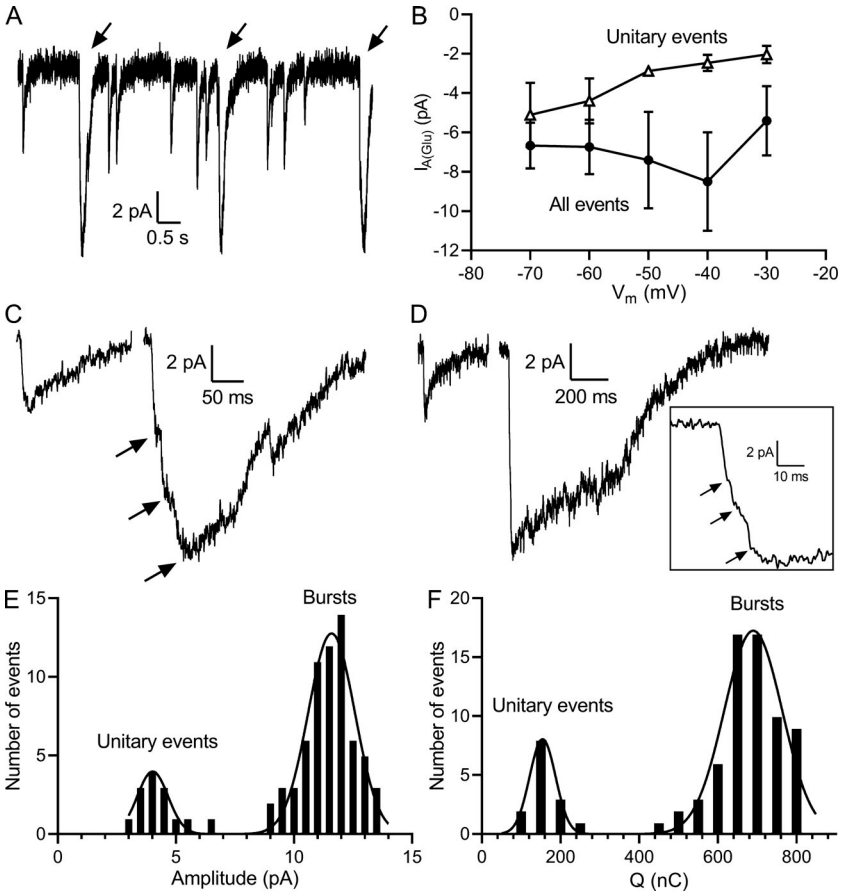

Figure 3. **Bursts are multiples of unitary events. (A)** Example trace of burst events (arrows) along with unitary events at −40 mV. This record was chosen for an abundance of unitary events. **(B)** The amplitude of single-vesicle unitary events (n = 6 rods) decreased with depolarization (open triangles). When the amplitude of all events from the rod shown in A were plotted together, event amplitude initially increased as more vesicles were released in bursts and then diminished with further depolarization and a further decrease in driving force. **(C)** Comparing waveforms of unitary and burst events in cells held at −40 mV indicates that bursts are due to sequential fusion of multiple vesicles. The initial inward current during a burst (right) typically showed multiple inflection points occurring at intervals similar to the amplitude of unitary events (left). **(D)** On a slow time base, this burst (right) appeared to show a smooth rising phase, but when examined at higher time resolution (inset), one can see three inflection points (arrows in C and D) that are roughly the same size as a unitary event in the same cell (left). **(E)** Amplitude frequency distribution of unitary and burst events from the rod shown in A when voltage was clamped at −40 mV. Multiple Gaussian fit with means of 4.0 ± 0.7 and 11.7 ± 1.0 pA (mean ± SD). **(F)** Charge transfer frequency distribution from the same cell suggested that each burst consisted of approximately five vesicles. Multiple Gaussian fit yielded means of 154.5 ± 32.9 and 689.9 ± 73.8 nC (error bars show mean ± SD). Q, quanta.

showed two discrete peaks, one representing unitary events with a mean amplitude of 4.0 ± 0.7 pA and the other representing bursts with a mean amplitude of 11.7 ± 1.0 pA. Fig. 3 F plots the frequency distribution for charge transfer measurements of the same set of bursts and unitary events. A multiple Gaussian fit yielded a mean amplitude for unitary events of 154.5 ± 32.9 nC with bursts averaging 689.9 ± 73.8 nC. Thus, in this example, the amplitude of bursts was threefold larger than the single-quantal amplitude, but the charge transfer of bursts was fivefold larger than the single-vesicle charge transfer. This suggests that the bursts in this example consisted of an average of approximately five vesicles apiece. Bursts more often (81%; n = 22 cells) consisted of 10–20 vesicles with an apparent upper limit of 45–60 vesicles (3%; n = 22 cells). Quanta per burst calculated from charge transfer (17 ± 7; n = 22 rods) was always larger than the ratio of bursts to unitary events calculated from amplitude measurements (3 ± 1; P < 0.0001, n = 22 cells, t test). The time constant for decline was also two to three times slower for bursts (bursts, τ = 164.4 ± 49.8 ms, n = 31) than unitary events (τ = 71.9 + 40.7 ms, n = 29; P < 0.0001, unpaired t test). Together, these data indicate that multiple vesicles were released sequentially during each burst.

Cones do not show bursting

Cones voltage clamped at −40 mV did not show the same bursting behavior seen in rods, but instead showed both small and large individual release events with uniform kinetics, suggesting a more synchronous form of multiquantal release (Fig. 4). The example recordings and amplitude histogram in Fig. 4, A and B, show evidence for numerous large events along with many more small events in a rod held at −70 mV. Fig. 4, C and D, shows the amplitude histogram and response waveforms of release events measured in the same rod held at −40 mV. The insets show examples of large events measured at −70 (Fig. 4 A) and −40 mV (Fig. 4 C). Large and small events showed uniform kinetics, suggesting that large events arose from the synchronized fusion of multiple vesicles. As shown in Fig. 4, A and B, large multiquantal events were even seen during spontaneous release in cones held at −70 mV. These results differed from those in rods where multiquantal release was sequential, not synchronous, and only emerged at more depolarized potentials. Comparing events measured at −40 mV with those measured at −70 mV, the overall amplitude distribution showed a significant rightward shift to more positive values (Kolmogorov-Smirnov test, P = 0.006), despite the decrease in anion driving force at −40 mV (Fig. 4 C). This suggests that the number of multiquantal release events also increased with depolarization. Unitary events had a faster 10–90% rise time (7.4 ± 5 ms, n > 40 events in 3 cells, 3 animals) in cones than in rods (9.3 ± 1.3 ms, n = 12 rods, 9 animals; P < 0.001, t test), suggesting a faster rise in synaptic cleft glutamate. The decay time constant (49.8 ± 79.6 ms, n > 40 events in 3 cells), which is shaped by the glutamate transporter cycle time, did not differ significantly from that of unitary events in rods (P = 0.33, t test). These data show that the

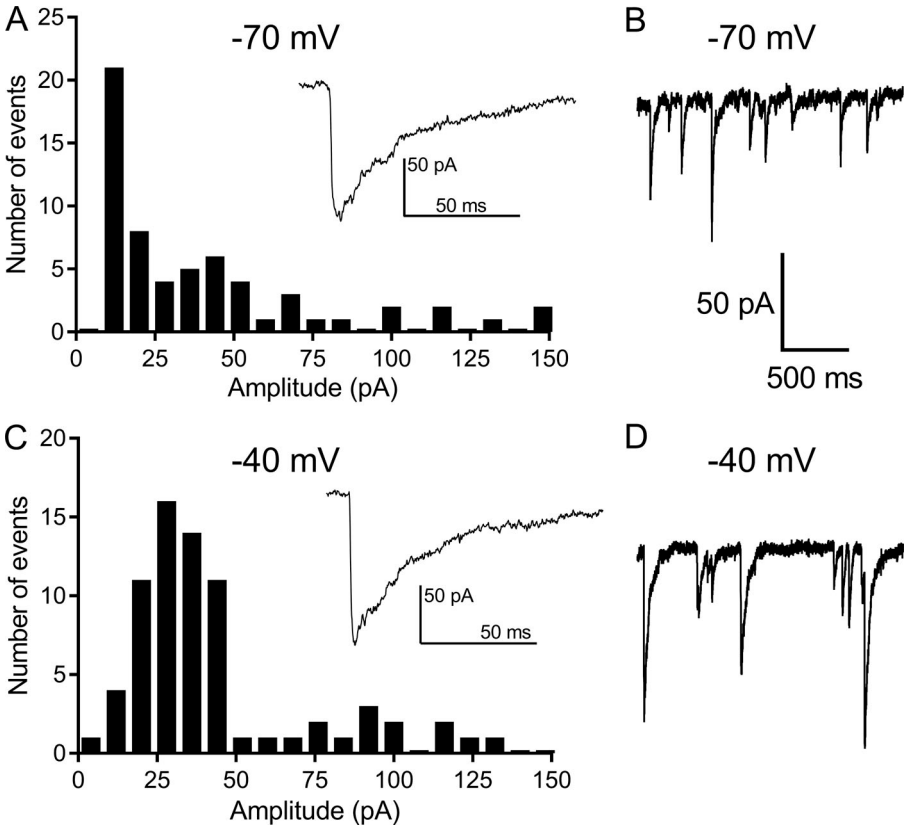

Figure 4. **Bursting appears to be a characteristic exclusive to rods. (A)** Amplitude histogram of spontaneous $I_{A(glu)}$ release events recorded in a cone voltage clamped at −70 mV (n = 61 events; mean amplitude, 36.8 ± 36.0 pA). Inset shows the waveform of a single spontaneous multiquantal release event. **(B)** Example recording of spontaneous events from the same cone held at −70 mV. **(C)** Amplitude histogram of spontaneous $I_{A(glu)}$ release events recorded in a cone voltage clamped at −40 mV (n = 72 events; mean amplitude, 42.1 ± 28.8 pA) shows the presence of numerous large events. The waveform of a synchronous multiquantal release event at −40 mV (inset) showed the same kinetics as events measured at −70 mV, suggesting a more synchronized mechanism of multivesicular release than in rods. **(D)** Example recording of spontaneous events from the same cone held at −40 mV. The presence of many large events in the example traces suggest cones are capable of synchronous release of multiple vesicles.

bursting behavior is specific to rods, suggesting it may play a role in signaling information under dim light conditions.

Vesicle pools involved in bursting

The number of quanta in each burst was sensitive to the length of the prior interburst interval. The example trace in Fig. 5 A shows a 30-s series of bursts. While bursts were relatively stereotyped in amplitude and duration, the arrow points to a slightly larger burst that followed a longer-than-average interval. The number of quanta in each burst is plotted against the interburst interval in the graph below. The filled red circles show data points from the example trace. The other data points came from 14 additional 30-s recordings in the same rod. When fit by linear regression, the slope of the straight line was significantly greater than zero (n = 12 rods), with an average correlation coefficient of r^2 = 0.29 (n = 12). While bursts generally increased in size with longer interevent intervals, they typically reached a plateau of 15–20 vesicles per burst.

Bursts in rods held steadily at −40 mV and release events evoked by brief, strong depolarizing stimuli originated from an overlapping pool of vesicles. With a strong depolarizing test step (25 ms, −70 to −10 mV) designed to release the entire readily releasable pool, release events averaged 21 ± 12 vesicles (n = 9) as measured from $I_{A(glu)}$ charge transfer following termination of the step. Some bursts were larger than evoked responses, but some were also smaller, and there was no significant difference between the number of quanta in evoked responses and bursts (17 ± 7, n = 22 rods, n = 15 animals; P = 0.17, unpaired t test).

To compare vesicle pools involved in these two forms of release more directly, we tested for cross-depletion. To do so, we voltage clamped rods at −40 mV for 30 s, then applied a brief depolarizing step to −10 mV (25 ms) to deplete the releasable pool, and finally returned the membrane potential to −40 mV for another 30 s. In a few cells, including the cell illustrated in Fig. 6 A, we held cells at −30 mV to evoke more vigorous bursting. As shown in Fig. 6 A, the depolarizing step to −10 mV evoked an inward current that was similar in size and shape to bursts that occurred before and after the step. In the next trial, a burst occurred immediately before the step to −10 mV, and the depolarizing step failed to evoke release (Fig. 6 B). We defined a quantal ratio as the charge transfer in each burst relative to the charge transfer evoked by the step. We measured this ratio for bursts immediately preceding and following the step. The quantal ratio before the step was significantly >1 (1.475 ± 0.680, n = 32; P = 0.0004, one-sample t test), consistent with idea that the preceding burst depleted vesicles from the pool available for a subsequent evoked response. After the step, there was a pause of ∼500 ms during which no bursts were observed. Burst ratios then remained <1 for another 1 s. This is consistent with the previous experiment showing that burst size increased with interburst intervals, at least up to a point. Together, these data suggest that bursts involve a vesicle pool that significantly overlaps with the readily releasable pool of vesicles evoked by strong depolarizing steps.

Bursts depend on calcium

The rate of release increased in parallel with the voltage-dependent increase in I_{Ca}, suggesting it was Ca^{2+} dependent. The essential role of Ca^{2+} influx was confirmed by adding the

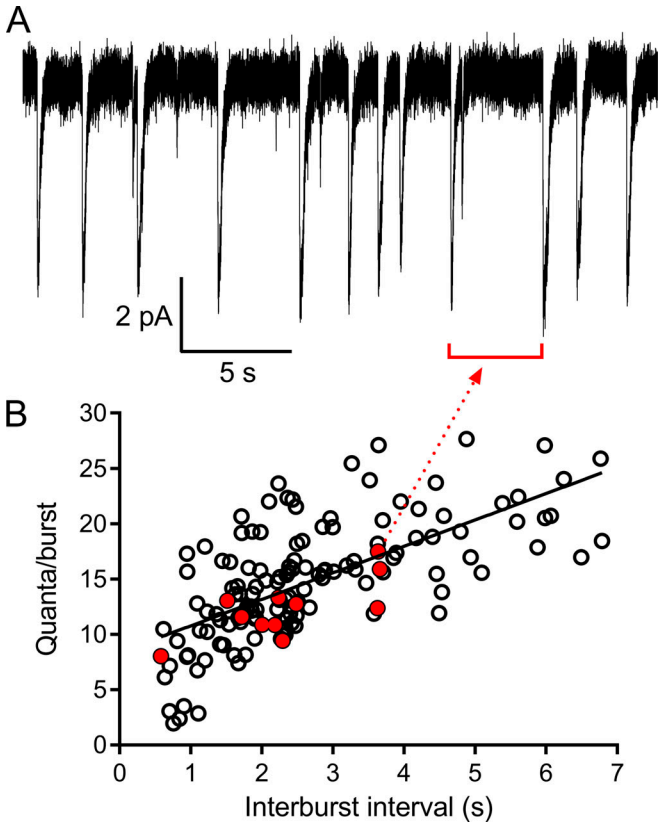

Figure 5. **Longer intervals preceded larger bursts in rods. (A)** Example of a series of bursts in a rod held at −40 mV for 30 s. While the bursts were similar in amplitude and duration to one another, longer interburst intervals typically preceded larger bursts. The arrow points to the largest burst in this trace and its corresponding measurement in the graph. **(B)** Plot of the number of quanta per burst versus the preceding interval. To assess the number of quanta per burst, we measured the burst charge transfer and then divided that value by the uniquantal charge transfer for spontaneous events at the same potential. The circles show data from 15 recordings (30 s apiece) in the same rod. The filled red circles show the data points from the example trace. The linear regression fit to all 158 data points showed a significant slope of 2.39 ± 0.23 quanta/burst/s (P < 0.0001, F-test) with a correlation coefficient (r^2) of 0.43. Linear regression to data from the record shown in A (red filled circles; n = 11) showed a slope of 2.10 ± 0.61 (P = 0.0075) with r^2 = 0.57 (not shown).

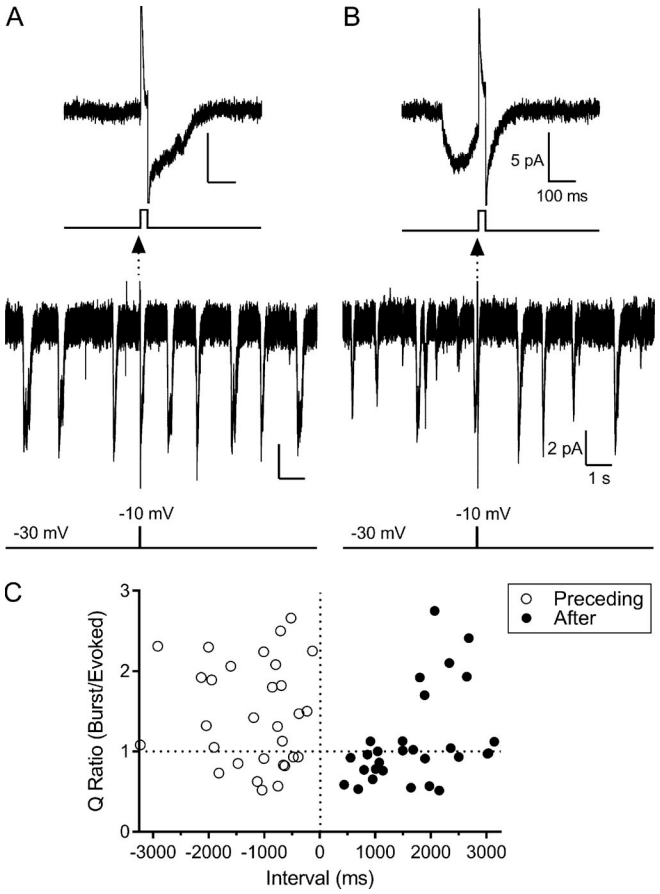

Figure 6. **Cross-depletion experiments suggest that bursts involve the readily releasable pool of vesicles released by brief depolarizing steps. (A)** A rod was voltage clamped at −30 mV and then stepped briefly to −10 mV to empty the readily releasable pool. The $I_{A(glu)}$ release event evoked by the 25-ms step to −10 mV was similar in amplitude and duration to surrounding burst events. **(B)** In the next trial in the same rod, evoked release was not observed when a burst immediately preceded the step to −10 mV, suggesting a shared vesicle pool. **(C)** The quantal (Q) ratio is the number of vesicles in each burst relative to the number of vesicles evoked by a 25-ms depolarizing step from −30 or −40 mV to −10 mV. We calculated the Q ratio for bursts immediately before (n = 32 experiments in 12 rods) and after the test step (n = 34). Before the test step, the Q ratio was generally larger than unity, consistent with depletion by the preceding burst of the pool accessed during evoked release. Following the step, there was a pause of 500 ms, and then the Q ratio remained <1 for the next 1 s. This suggests that the prior step depleted the vesicles available for bursting. Dotted vertical line indicates time of the depolarizing stimulus pulse. Dotted horizontal line denotes a Q ratio of 1.

voltage gated Ca^{2+} channel blocker Cd^{2+} to the external solution (n = 3 rods, 2 animals; Fig. 7, A and B). This eliminated bursting, but some unitary release events persisted even in the presence of Cd^{2+} at all potentials, suggesting they arise by Ca^{2+}-independent spontaneous release from rods, similar to spontaneous release in salamander rods (Cork et al., 2016; Hays et al., 2020).

As shown in Fig. 2 C, the membrane voltage of −40 mV approaches the midpoint activation voltage for rod I_{Ca} (Babai and Thoreson, 2009), so we investigated whether increasing the open time of L-type Ca^{2+} channels extended burst duration by recruiting additional vesicles. Lengthening Ca^{2+} channel openings by bath application of BayK8644 (2 µM; Koschak et al., 2003) did not significantly alter release properties at −40 mV. Bursts consisted of 22.2 ± 6.7 vesicles in control conditions compared with 19.6 ± 9.8 vesicles in BayK8644 (P = 0.24, n = 4 cells, 2 animals, paired t test). Burst event duration was also unchanged by extending Ca^{2+} channel open times (control half-width was 217.8 ± 30.6 ms versus 185.5 ± 45.5 ms in BayK8644; P = 0.4, paired t test, n = 4 cells). The frequency of individual uniquantal events in periods of 30 s (12.3 ± 13.8 events) was also not changed by BayK8644 treatment (12.3 ± 11.7 events, n = 4 rods; P = 0.2, paired t test). Thus, overall release rates at −40 mV were not increased with BayK8644 treatment (Fig. 7 C). These data suggest that while the initial influx of Ca^{2+} through Ca^{2+} channels is required to trigger a burst, the number of vesicles in each burst is not strongly shaped by further influx and diffusion of Ca^{2+} from voltage-gated Ca^{2+} channels. Evidence that no

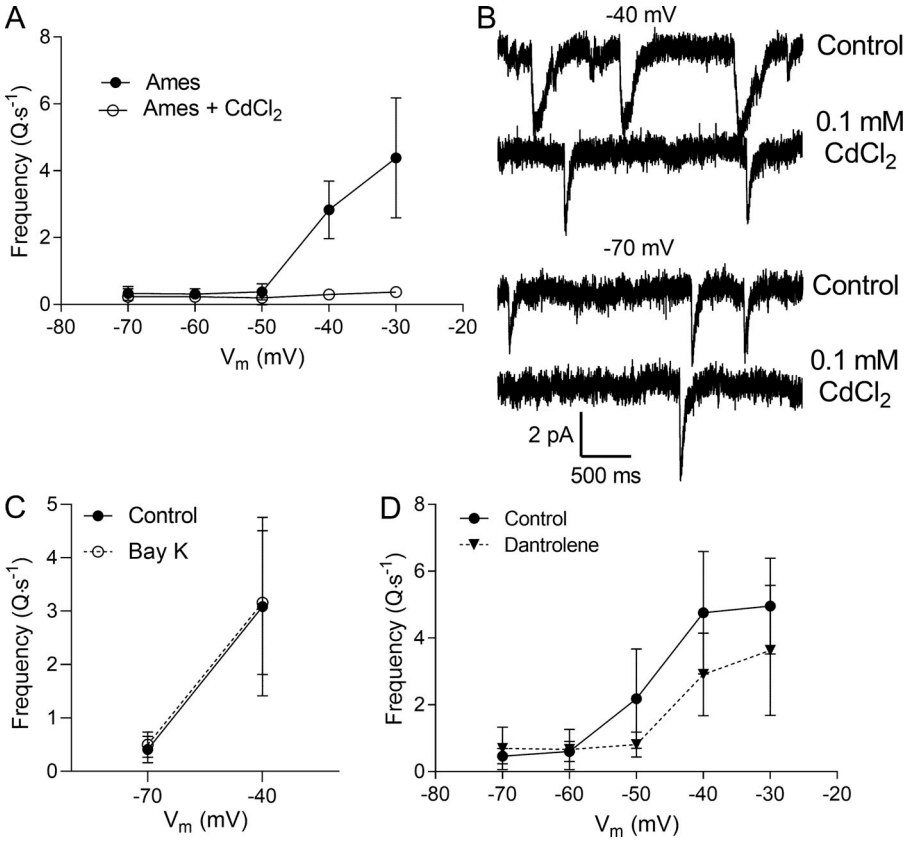

Figure 7. **Bursting requires Ca^{2+} from voltage-gated Ca^{2+} channels. (A)** Plotting the rate of release in control and $CdCl_2$ (0.1 mM) measured in the same three rods (P = 0.0009, two-way ANOVA). **(B)** Example traces in control and $CdCl_2$ at −40 and −70 mV. Including $CdCl_2$ in the extracellular medium abolished bursts of release at depolarized potentials, but Ca^{2+}-independent spontaneous, unitary release events remained. **(C)** Including BayK8644 (2 µM) in the extracellular solution did not increase release rates measured at −70 or −40 mV (P = 0.96, two-way ANOVA; *n* = 4 rods, 2 animals). **(D)** Inclusion of an RYR inhibitor, dantrolene (100 µM), in the pipette solution modestly reduced overall release frequency (control, *n* = 9 rods; dantrolene, *n* = 7 rods, 2 animals; P = 0.006, two-way ANOVA). Error bars show mean ± SD. V_m, membrane voltage.

additional vesicles are available for release is consistent with the hypothesis that bursts empty the entire readily releasable pool (Thoreson et al., 2016).

Results from mouse and salamander retina have shown that Ca^{2+} released from internal stores by CICR promotes release when rods are tonically depolarized (Babai et al., 2010a; Cadetti et al., 2006; Suryanarayanan and Slaughter, 2006). Consistent with this, we found that blocking CICR by introducing an RYR inhibitor, dantrolene (100 µM), through the patch pipette caused a modest reduction in release rates (P = 0.006, mixed model ANOVA; Fig. 7 D). However, CICR was not required for coordinating bursts, because they persisted after introducing dantrolene or a high concentration of ryanodine (100 µM) into rods through the patch pipette (*n* = 4; Fig. S1; see text at bottom of the PDF). The replenishment of internal stores by store-operated channels also does not appear necessary for bursts, because application of the Orai/Stim1 blocker SKF96368 (10 µM) through the patch pipette did not eliminate bursting behavior (Fig. S1; n = 3 rods, 1 animal). We also tested whether feedback from horizontal cells to rods might be responsible for organizing bursts, but bursts at −40 mV appeared to be unchanged by bath application of 10 µM α-amino-3-hydroxy-5-methyl-4-isoxazolepropionic acid (AMPA) receptor blocker 2,3-dioxo-6-nitro-7-sulfamoyl-benzo[f]quinoxaline (NBQX; Fig. S1; n = 3 rods, 1 animal).

We manipulated intracellular Ca^{2+} buffering to probe the spatiotemporal Ca^{2+} distribution controlling release rates and bursting behavior. Typically, our pipette solution contained 5 mM EGTA as the principal Ca^{2+} buffer. Replacing EGTA with the faster Ca^{2+} buffer, 1,2-bis(*o*-aminophenoxy)ethane-*N*,*N*,*N*′,*N*′-tetraacetic acid (BAPTA), reduced the voltage-dependent increase in release rates. The reduction in rate was similar with both 1 and 10 mM BAPTA (P = 0.0004, *n* = 5–8, mixed model ANOVA; Fig. 8), but neither concentration totally eliminated bursting at −40 mV. Buffering Ca^{2+} with 10 mM BAPTA eliminated $I_{A(glu)}$ evoked by strong depolarizing steps (25 ms; −70 to −10 mV; 1.04 ± 0.271 pA; *n* = 3 rods, 3 animals) compared with 5 mM EGTA (9.88 ± 1.77 pA; *n* = 16 rods, 14 animals; P = 0.049, unpaired *t* test), showing that BAPTA successfully reached the terminal during whole-cell recording. The number of quanta in each burst was unchanged by either concentration of BAPTA (5 mM EGTA, 17 ± 7, *n* = 22 cells; 1 and 10 mM BAPTA, 13 ± 4 and 11 ± 7; *n* = 5 cells each; P = 0.1289, one-way ANOVA). However, switching from EGTA to BAPTA lengthened the intervals between burst events from 2,756 ± 596 in control conditions with 5 mM EGTA (*n* = 14 cells) to 4,805 ± 1,524 ms with 1 mM BAPTA (P = 0.02, ANOVA; *n* = 5 cells, 3 animals) and 6,523 ± 2,535 with 10 mM BAPTA (P = 0.008, ANOVA; *n* = 4 cells, 3 animals). The number of unitary events between bursts was not reduced by 1 or 10 mM BAPTA buffering (10 mM; P = 0.6, *t* test; *n* = 5 cells of each condition), consistent with other evidence that these events result from Ca^{2+}-independent spontaneous release. Large Ca^{2+}-dependent Cl^- currents could sometimes be activated during maintained depolarizing stimulation even after strong buffering with 10 mM BAPTA, suggesting that Ca^{2+} buffers may become saturated by the continued influx of Ca^{2+} during 30-s steps (Fig. S2). Nevertheless, the ability of bursts to persist in the presence of strong and fast buffering by

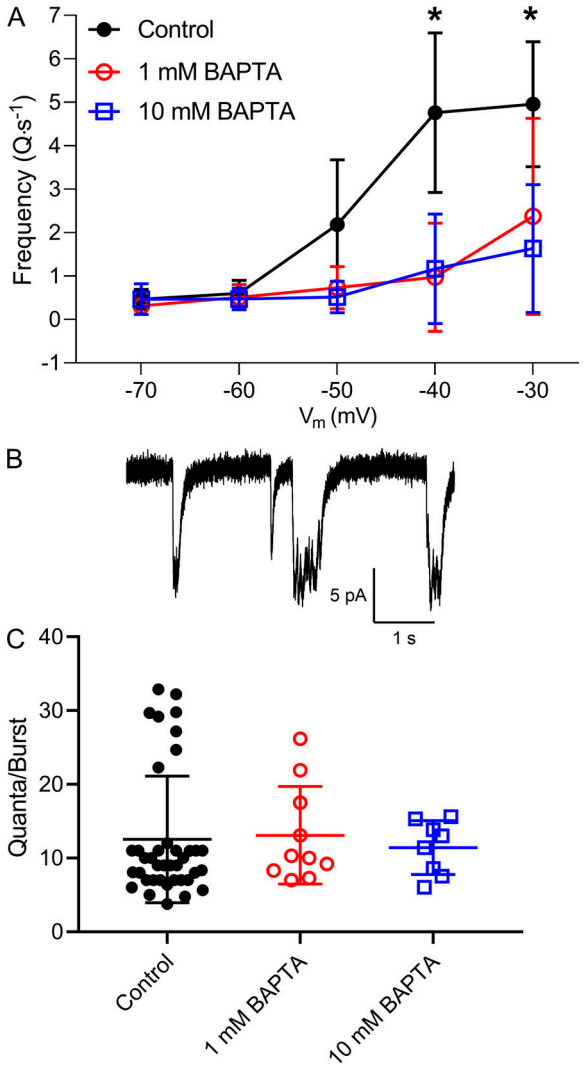

Figure 8. **Replacing EGTA in the patch recording pipette with the faster Ca^{2+} buffer BAPTA reduced release rates during 30-s steps (P = 0.0004, two-way ANOVA). (A)** Release rate was reduced by 1 mM BAPTA compared with 5 mM EGTA at −40 mV (P = 0.004, two-way ANOVA, Tukey's multiple comparisons). 10 mM BAPTA significantly reduced release rates at −40 and −30 mV (P < 0.01, two-way ANOVA, Tukey's multiple comparisons test; 5 mM EGTA, *n* = 8 rods [same data as control data in Fig. 6 D]; 1 mM BAPTA, *n* = 5; 10 mM BAPTA, *n* = 5). **(B)** Trace illustrating bursting in a rod when intracellular Ca^{2+} was buffered with 10 mM BAPTA. **(C)** Buffering by 1 mM (*n* = 10 rods) or 10 mM (*n* = 8 rods) BAPTA did not eliminate bursting, and bursts consisted of the same number of quanta as the control (control, *n* = 22 rods; control versus 1 mM BAPTA, P = 0.62; control versus 10 mM BAPTA, P = 0.13; one-way ANOVA, Tukey's multiple comparisons test). Error bars show mean ± SD. *, P < 0.05; unpaired *t* tests.

BAPTA suggests they involve release sites very close to ribbon-associated Ca^{2+} channels.

Ca^{2+} sensor Syt1 is required for bursting

We next tested how the Ca^{2+} sensor Syt1 shapes sustained release. Selective elimination of Syt1 from mouse rods abolishes fast, synchronous, Ca^{2+}-dependent exocytosis evoked by brief depolarizing steps, although some slower release remains, suggesting the presence of another sensor (Grassmeyer et al., 2019). Elimination of Syt1 also elevated the rate of spontaneous release in rods voltage clamped at −70 mV (Grassmeyer et al., 2019). This is consistent with evidence from other systems that Syt1 helps to clamp the SNARE apparatus and prevent spontaneous fusion (Courtney et al., 2019; Grushin et al., 2019; Xu et al., 2009). Along with an increase in spontaneous release at −70 mV (Fig. 9; 0.45 ± 0.23 events/s in control mouse rods, *n* = 8, 4 animals, versus 4.2 ± 2.3 events/s in mouse rods lacking Syt1, *n* = 9, 5 animals; P < 0.001, *t* test), we saw a further small increase in release rates with depolarization above −50 mV in rods lacking Syt1. The small voltage-dependent increase in release at −40 and −30 mV that remained after eliminating Syt1 from rods was abolished by replacing 5 mM EGTA with 1 mM BAPTA in the patch pipette (Fig. 9 B). This suggests that this residual release may involve nonribbon release sites that use a different Ca^{2+} sensor (Grassmeyer et al., 2019). Above −50 mV, roughly the same number of quanta were released over long periods of time (30 s) as in control rods, but events in rods lacking Syt1 were largely uniquantal and not organized in bursts (Fig. 9 A). Fig. 9, C and D, plots the frequency distribution for charge transfer measurements in a rod voltage clamped at −70 and −40 mV. Unlike control rods that showed a bimodal distribution of charge transfer when held at −40 mV (Fig. 3), rods lacking Syt1 showed a unimodal distribution at both −70 and −40 mV (Fig. 9, C and D). Furthermore, the mean single-event charge transfer was smaller at −40 mV (−396 ± 175 nC; *n* = 75 events) than at −70 mV (−577 ± 180 nC; *n* = 48 events). This suggests that unclamping Syt1 may facilitate fusion of vesicles that would normally be released only after an increase in Ca^{2+} and that the clamping function of Syt1 may be necessary to maintain inactive periods between bursts, allowing accumulation of a sufficient number of vesicles to initiate a burst at −40 mV.

Discussion

An appreciation of the mechanisms underlying tonic release of glutamate-containing vesicles from rods, graded by membrane potential, is critical to understanding how synaptic transmission is regulated by light-evoked changes in rod membrane potential. Using $I_{A(glu)}$ to assay release from individual rods, we measured the voltage-dependent increase in glutamate release at individual rod ribbon synapses. Release rates rose gradually in parallel with the voltage-dependent increase in I_{Ca}, attaining a rate of ∼11 vesicles/s (35°C) at the typical resting potential in darkness of −40 mV. Along with this increase in rate, the nature of release changed, shifting from uniquantal release at −70 mV to coordinated bursts of vesicles at −40 mV. In this study, we explored the mechanisms underlying these different components of release.

Temperature dependence of release

Our results showed a linear dependence of release on I_{Ca}, similar to earlier results in amphibian rods (Thoreson et al., 2004). Voltage-dependent changes in glutamate release rate tracked with I_{Ca} even when the temperature of the system was increased to physiological levels. Fusogenicity of the SNARE complex employed by rods for exocytosis is controlled by entropic forces, so complex formation and zippering are not aided by increases

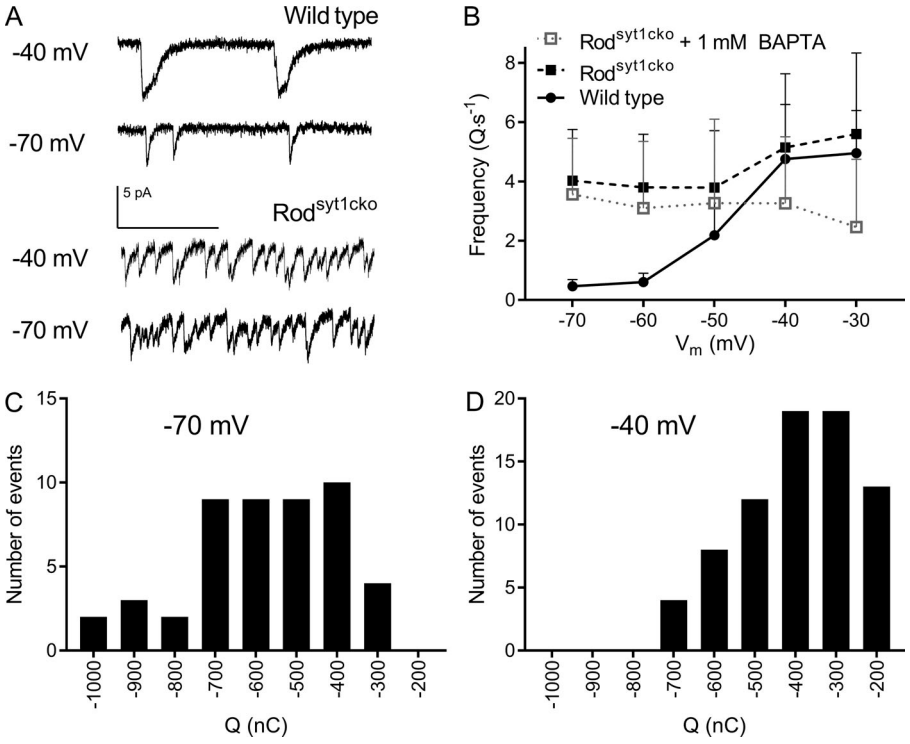

Figure 9. **Syt1 is required for bursting at −40 mV. (A)** Representative traces at −40 and −70 mV illustrate the differences in release characteristics in wild-type and Syt-conditional knockout rods ($Rod^{syt1cko}$). Selective elimination of Syt1 from rods eliminated bursting and increased the rate of spontaneous unitary events. **(B)** After Syt1 elimination (n = 9 rods, 5 animals), vesicle release rates were increased. Further voltage-dependent increases in release rates at −40 and −30 mV remained but were reduced in Syt1CKO rods by using the fast Ca^{2+} buffer BAPTA (1 mM; n = 8 rods, 4 animals) rather than EGTA (5 mM; n = 9 rods, 5 animals). **(C)** Frequency histogram for charge transfer measurements in a Syt1CKO rod voltage clamped at −70 mV. Mean, −577 ± 180 nC; n = 48 events. **(D)** Frequency histogram for charge transfer measurements in the same rod voltage clamped at −40 mV. Mean, −396 ± 175 nC; n = 75 events. Error bars show mean ± SD. Q, quanta.

in temperature (Mostafavi et al., 2017). Thus, rate appears to depend chiefly on the increase in I_{Ca} that accompanies increasing temperature with Q_{10} = 2.1. Voltage-gated Ca^{2+} channels in rods are L-type channels containing $Ca_V1.4$, with several splice variants that have different kinetics and gating properties (Haeseleer et al., 2016; Tan et al., 2012). While the gating properties of some voltage-gated ion channels are strongly temperature dependent (Q_{10} = 5–10; DeCoursey and Cherny, 1998; Hille, 2001; Lee and Deutsch, 1990), our experiments agree with the relatively weak temperature dependence of $Ca_V1.4$ (Q_{10} = 2–4) measured in various systems (Allen, 1996; Herve et al., 1992; Hope et al., 2005). Studies of synaptic release in bullfrog inner hair cells that also contain synaptic ribbons and employ L-type Ca^{2+} channels (Brandt et al., 2005) describe a stronger temperature dependence of release frequency but agree with the present study in that increases in release are likely due to enhanced ion currents rather than changes in the fusion machinery itself (Chen and von Gersdorff, 2019; Sabatini and Regehr, 1996). It is possible that other parts of the synaptic vesicle cycle are accelerated by temperature, but the large reservoir of cytoplasmic vesicles makes rods less immediately reliant on fast endocytosis for refilling the readily releasable pool (von Gersdorff and Matthews, 1997). The tight relationship between release and Ca^{2+} influx improves linearity in the transformation of light-evoked changes in membrane potential into synaptic release.

Spontaneous release

Spontaneous release can be important for circuit development, synaptic plasticity, and shaping spiking patterns (Andreae et al., 2012; Carter and Regehr, 2002; McKinney et al., 1999). At a hyperpolarized potential of −70 mV, where Ca^{2+} channels are minimally active, spontaneous release rates were slow, with rates of 0.45 ± 0.24 Hz at room temperature and 0.7 ± 0.6 Hz at 35°C. This is similar to rates of Ca^{2+}-independent release in amphibian rods and cones of 1.3 vesicles/s/ribbon and 0.8–0.9 vesicles/s/ribbon (Cork et al., 2016; Hays et al., 2020). Spontaneous release can be triggered by the stochastic opening of L-type Ca^{2+} channels, but vesicles can also be released from salamander rods independent of Ca^{2+} influx (Cork et al., 2016). Our results show that mouse rods are capable of Ca^{2+}-independent spontaneous release, since strong buffering by 10 mM BAPTA or inclusion of $CdCl_2$ in the extracellular medium did not eliminate spontaneous fusion events.

The increase in spontaneous release rates observed in Syt1-knockout rods is consistent with the hypothesis that Syt1 serves as a fusion clamp (Courtney et al., 2019). In the absence of Syt1, we observed a slight increase in release rates above −50 mV that was depressed by introducing the fast Ca^{2+} buffer BAPTA into rods. This suggests that the enhanced spread of Ca^{2+} that accompanies strong stimulation may recruit more distant release sites that use a different Ca^{2+} sensor. Syt7 and Doc2 have both been proposed as sensors for slower asynchronous release that is not tightly coupled to Ca^{2+} channel openings (Bacaj et al., 2013; Chung et al., 2010; Luo et al., 2015; Turecek and Regehr, 2018; Yao et al., 2011). Doc2 has also been proposed to be a sensor for spontaneous release (Pang et al., 2011; Ramirez et al., 2017; Yao et al., 2011), and RNA-sequencing experiments show high levels of Doc2B mRNA in rods (Kim et al., 2016).

Bursting behavior

Our data showed that while spontaneous release from rods held at −70 mV involved the stochastic release of individual vesicles, depolarizing rods to −40 mV caused the emergence of

multiquantal bursts of release consisting of 10–20 vesicles apiece. In addition to their voltage dependence, bursts were blocked by Cd^{2+}, indicating that they required Ca^{2+} influx through voltage-dependent Ca^{2+} channels. Furthermore, bursting at −40 mV was absent from rods lacking the exocytotic Ca^{2+} sensor Syt1 (Grassmeyer et al., 2019). While other Ca^{2+} sensors may also be present in rods and participate in coordinating bursts, it is clear that Syt1 is absolutely essential. The loss of Syt1 may directly interrupt bursting or act indirectly by depleting an overlapping pool of vesicles; nevertheless, these results indicate that the vesicles involved in bursting are released by Syt1-mediated mechanisms. In addition, because I_{Ca} and passive membrane properties were unchanged in rods lacking Syt1 (Grassmeyer et al., 2019), the absence of bursting in these cells with the same basic biophysical properties indicates that bursts were not due to a loss of voltage-clamp and regenerative activation of I_{Ca}.

Inclusion of 10 mM BAPTA in the patch pipette did not abolish the bursting that accompanied maintained depolarization. The persistence of bursts in the presence of BAPTA suggests that they involve release sites within Ca^{2+} nanodomains extremely close to Ca^{2+} channels. Since Ca^{2+} channels are clustered beneath ribbons (Lv et al., 2012; Mercer et al., 2011; Morgans, 2001; Specht et al., 2009), this in turn suggests that ribbon-associated vesicles participate in bursting. While the buffering capacity could be overwhelmed by the continued influx of Ca^{2+} during prolonged depolarizing stimulation, the cross-depletion between vesicle pools involved in bursts and depolarization-evoked release, along with evidence that the number of vesicles in bursts matched the number of vesicles released by a brief strong depolarizing step, suggests that the pool of vesicles involved in bursts overlaps considerably with the readily releasable pool of vesicles, which is thought to reflect vesicles tethered at the base of the ribbon (LoGiudice and Matthews, 2009; Mennerick and Matthews, 1996).

Unlike the bursting in rods that involved sequential fusion of vesicles, release events in cones varied widely in amplitude, but large events exhibited the same kinetics as small events, suggesting large events are due to the synchronized fusion of multiple vesicles. One aspect of release that differs between the two cell types is that rods, but not cones, are capable of release at nonribbon sites triggered by CICR (Babai et al., 2010b; Cadetti et al., 2006; Chen et al., 2014; Chen et al., 2015). The capability of nonribbon release in rods is akin to nonribbon release driven by global Ca^{2+} changes in retinal bipolar cells (Mehta et al., 2014). We examined whether CICR was necessary to coordinate bursting but found that bursts were not abolished by the CICR inhibitor dantrolene, blocking RYRs with a high concentration of ryanodine, or use of a store-operated channel inhibitor. These data suggest that release of Ca^{2+} from stores is not required for bursting behavior. We also considered the idea that bursts required the coincident opening of a certain number of Ca^{2+} channels. However, the intervals between bursts are not likely to be due to cessation of Ca^{2+} influx since $Ca_V1.4$ channels show minimal inactivation. If we assume a single-channel current of 0.3 pA (Bartoletti et al., 2011; Brandt et al., 2005), the amplitude of I_{Ca} at −40 mV suggests that seven or eight channels should be open at any given moment. Furthermore, lengthening Ca^{2+} channel openings with the dihydropyridine agonist BayK8644 did not reduce interburst intervals or extend burst durations. The finding that the increase in Ca^{2+} influx accompanying treatment with BayK8644 did not lengthen bursts is also consistent with the idea that each burst empties the entire pool of vesicles available for immediate release (Thoreson et al., 2016).

The finding that larger bursts were generally preceded by longer interburst intervals and evidence from cross-depletion experiments both suggest that bursts are shaped by vesicle replenishment kinetics. Ca^{2+} speeds replenishment at rod and cone ribbon synapses (Babai et al., 2010a; Van Hook et al., 2014; Van Hook and Thoreson, 2015), so the finding that inhibiting CICR with dantrolene slowed release rates is consistent with a role for Ca^{2+} in speeding replenishment. Interburst intervals were also extended by BAPTA, consistent with a slower rate of replenishment with less available intracellular Ca^{2+} (Babai et al., 2010a; Van Hook et al., 2014; Van Hook and Thoreson, 2015). Inhibiting calmodulin slows replenishment in rods and cones (Van Hook et al., 2014; Van Hook and Thoreson, 2015). Interactions between calmodulin and the Ca^{2+} sensor Syt7 can also regulate replenishment (Liu et al., 2014).

Burst sizes appear constrained by the number of vesicles available for release. While bursts were initiated by fusion of a few vesicles at the base of the ribbon located within Ca^{2+} channel nanodomains, the release of subsequent vesicles during the burst involved sequential fusion of additional vesicles. The sequential nature of vesicle fusion during these bursts looks superficially similar to multiquantal release in hair cells (Grant et al., 2010). In hair cells, it has been suggested that complex kinetics of release events arise from flickering of fusion pores (Chapochnikov et al., 2014). In our hands, unitary $I_{A(glu)}$ events at −70 mV were uniform in both kinetics and magnitude, suggesting full vesicle fusion, releasing one whole quantum during spontaneous release. The burst events at −40 mV consistently had larger charge transfer than spontaneous unitary events, so it seems unlikely that bursts originated from only a single vesicle.

Functional considerations

Bursting behavior was not observed previously in salamander rods, where multivesicular release instead involves synchronized fusion (Hays et al., 2020). Amphibians lack the rod bipolar cells that in mammals are specialized for transmitting rod light responses at scotopic threshold (Wu, 2010). Bursts were also not seen in cones of the mouse and salamander. These results suggest that bursts may have a particular role in transmitting scotopic signals. One strategy for achieving reliable transmission of single-photon responses at a rod synapse is to maintain extremely fast release rates; however, we found that release from rods at −40 mV and 35°C averaged only ∼11 vesicles/s/ribbon, substantially lower than the rate of ∼100 vesicles/s that is thought to be needed for reliable transmission, assuming a purely Poisson release process (Rao-Mirotznik et al., 1998; Rao et al., 1994; van Rossum and Smith, 1998). Our results in mouse rods are consistent with measurements made using the activity-dependent dye FM1-43, which showed release rates in darkness of 2.5 and 18 vesicles/s/ribbon from gecko and salamander rods,

respectively (Sheng et al., 2007). Maintaining a high rate of release during long periods of darkness requires a tremendous amount of energy and other cellular resources (Linton et al., 2010; Okawa et al., 2008; Yuan et al., 2018). An alternative strategy for making detection more reliable is to make release more regular and predictable (Schein and Ahmad, 2005; Schein and Ahmad, 2006). At the dark resting membrane potential of −40 mV, we consistently observed large multivesicular release events that occurred at semiregular intervals. The replenishment and delivery of vesicles to release sites at the base of each ribbon may help to make bursting occur at more regular intervals, and this may improve postsynaptic detection of single-photon responses.

To improve the detection of single photons at the synapse from rods, rod bipolar cells employ a nonlinear thresholding mechanism that filters out small signals that are more likely to arise from noise (Field and Rieke, 2002; Sampath and Rieke, 2004). To implement this thresholding mechanism, glutamate levels in the synaptic cleft must be maintained at high levels in darkness (Sampath and Rieke, 2004). The periodic release of many vesicles in a burst may provide a means of keeping glutamate levels high in rod synapses during darkness.

In summary, our results described several key factors that shape voltage-dependent changes in synaptic release of glutamate-filled vesicles from rods in the mouse retina. At negative membrane potentials normally achieved only with extremely strong illumination and where Ca^{2+} channels show little or no activity, individual synaptic vesicles are released sporadically in a Ca^{2+}-independent fashion. As Ca^{2+} channels open more frequently with increasing depolarization, vesicle release rates increase in parallel. However, the rate of vesicle release achieved at the typical resting potential in darkness of −40 mV remains slow, only ∼11 vesicles/s. At this membrane potential, release transitions from individual vesicle fusion events to coordinated bursts arising from the sequential fusion of 10–20 vesicles. These bursts involve the readily releasable pool of vesicles at the base of the ribbon and occur at more regular intervals than the stochastic fusion events seen at −70 mV. Intervals between bursts are shortened by elevating global Ca^{2+}, suggesting they are shaped by rates at which the releasable pool can be replenished. This is consistent with the idea that delivery of vesicles down the ribbon may provide a mechanism for regularizing release rates (Schein and Ahmad, 2005). Deletion of the exocytotic Ca^{2+} sensor Syt1 virtually eliminated voltage-dependent increases in sustained release at membrane potentials up to −40 mV. Consistent with effects of Syt1 deletion in cones (Grassmeyer et al., 2019), this indicates that kinetics of release at photoreceptor ribbon synapses are shaped more by kinetics of vesicle delivery to release sites at the ribbon base than by reliance on different release sites and different Ca^{2+} sensors as seen at many conventional synapses (Kaeser and Regehr, 2014).

Acknowledgments

Jeanne M. Nerbonne served as editor.

We thank Cody Barta for invaluable assistance with mouse husbandry.

Support was provided by a University of Nebraska Medical Center graduate fellowship to C.L. Hays and National Eye Institute grant EY10542 to W.B. Thoreson.

The authors declare no competing financial interests.

Author contributions: C.L. Hays and W.B. Thoreson planned the study, conducted experiments, analyzed data, and wrote the paper. A.L. Sladek conducted experiments and analyzed data.

Submitted: 24 July 2020
Revised: 1 October 2020
Accepted: 19 October 2020

References

Allen, T.J. 1996. Temperature dependence of macroscopic L-type calcium channel currents in single guinea pig ventricular myocytes. *J. Cardiovasc. Electrophysiol.* 7:307–321. https://doi.org/10.1111/j.1540-8167.1996.tb00532.x

Andreae, L.C., N.B. Fredj, and J. Burrone. 2012. Independent vesicle pools underlie different modes of release during neuronal development. *J. Neurosci.* 32:1867–1874. https://doi.org/10.1523/JNEUROSCI.5181-11.2012

Arriza, J.L., S. Eliasof, M.P. Kavanaugh, and S.G. Amara. 1997. Excitatory amino acid transporter 5, a retinal glutamate transporter coupled to a chloride conductance. *Proc. Natl. Acad. Sci. USA.* 94:4155–4160. https://doi.org/10.1073/pnas.94.8.4155

Babai, N., and W.B. Thoreson. 2009. Horizontal cell feedback regulates calcium currents and intracellular calcium levels in rod photoreceptors of salamander and mouse retina. *J. Physiol.* 587:2353–2364. https://doi.org/10.1113/jphysiol.2009.169656

Babai, N., T.M. Bartoletti, and W.B. Thoreson. 2010a. Calcium regulates vesicle replenishment at the cone ribbon synapse. *J. Neurosci.* 30:15866–15877. https://doi.org/10.1523/JNEUROSCI.2891-10.2010

Babai, N., C.W. Morgans, and W.B. Thoreson. 2010b. Calcium-induced calcium release contributes to synaptic release from mouse rod photoreceptors. *Neuroscience.* 165:1447–1456. https://doi.org/10.1016/j.neuroscience.2009.11.032

Bacaj, T., D. Wu, X. Yang, W. Morishita, P. Zhou, W. Xu, R.C. Malenka, and T.C. Südhof. 2013. Synaptotagmin-1 and synaptotagmin-7 trigger synchronous and asynchronous phases of neurotransmitter release. *Neuron.* 80:947–959. https://doi.org/10.1016/j.neuron.2013.10.026

Barnes, S., and M.C. Deschênes. 1992. Contribution of Ca and Ca-activated Cl channels to regenerative depolarization and membrane bistability of cone photoreceptors. *J. Neurophysiol.* 68:745–755. https://doi.org/10.1152/jn.1992.68.3.745

Bartoletti, T.M., S.L. Jackman, N. Babai, A.J. Mercer, R.H. Kramer, and W.B. Thoreson. 2011. Release from the cone ribbon synapse under bright light conditions can be controlled by the opening of only a few $Ca^{(2+)}$ channels. *J. Neurophysiol.* 106:2922–2935. https://doi.org/10.1152/jn.00634.2011

Baumann, L., A. Gerstner, X. Zong, M. Biel, and C. Wahl-Schott. 2004. Functional characterization of the L-type Ca^{2+} channel Cav1.4alpha1 from mouse retina. *Invest. Ophthalmol. Vis. Sci.* 45:708–713. https://doi.org/10.1167/iovs.03-0937

Behrens, C., T. Schubert, S. Haverkamp, T. Euler, and P. Berens. 2016. Connectivity map of bipolar cells and photoreceptors in the mouse retina. *eLife.* 5:e20041. https://doi.org/10.7554/eLife.20041

Berntson, A., and W.R. Taylor. 2003. The unitary event amplitude of mouse retinal on-cone bipolar cells. *Vis. Neurosci.* 20:621–626. https://doi.org/10.1017/S0952523803206040

Berntson, A., R.G. Smith, and W.R. Taylor. 2004. Transmission of single photon signals through a binary synapse in the mammalian retina. *Vis. Neurosci.* 21:693–702. https://doi.org/10.1017/S0952523804215048

Brandt, A., D. Khimich, and T. Moser. 2005. Few CaV1.3 channels regulate the exocytosis of a synaptic vesicle at the hair cell ribbon synapse. *J. Neurosci.* 25:11577–11585. https://doi.org/10.1523/JNEUROSCI.3411-05.2005

Cadetti, L., E.J. Bryson, C.A. Ciccone, K. Rabl, and W.B. Thoreson. 2006. Calcium-induced calcium release in rod photoreceptor terminals boosts synaptic transmission during maintained depolarization. *Eur. J. Neurosci.* 23:2983–2990. https://doi.org/10.1111/j.1460-9568.2006.04845.x

Cangiano, L., S. Asteriti, L. Cervetto, and C. Gargini. 2012. The photovoltage of rods and cones in the dark-adapted mouse retina. *J. Physiol.* 590:3841–3855. https://doi.org/10.1113/jphysiol.2011.226878

Carter, A.G., and W.G. Regehr. 2002. Quantal events shape cerebellar interneuron firing. *Nat. Neurosci.* 5:1309–1318. https://doi.org/10.1038/nn970

Chapochnikov, N.M., H. Takago, C.H. Huang, T. Pangršič, D. Khimich, J. Neef, E. Auge, F. Göttfert, S.W. Hell, C. Wichmann, et al. 2014. Uniquantal release through a dynamic fusion pore is a candidate mechanism of hair cell exocytosis. *Neuron.* 83:1389–1403. https://doi.org/10.1016/j.neuron.2014.08.003

Chen, M., and H. von Gersdorff. 2019. How to build a fast and highly sensitive sound detector that remains robust to temperature shifts. *J. Neurosci.* 39:7260–7276. https://doi.org/10.1523/JNEUROSCI.2510-18.2019

Chen, M., D. Križaj, and W.B. Thoreson. 2014. Intracellular calcium stores drive slow non-ribbon vesicle release from rod photoreceptors. *Front. Cell. Neurosci.* 8:20. https://doi.org/10.3389/fncel.2014.00020

Chen, M., M.J. Van Hook, and W.B. Thoreson. 2015. Ca^{2+} diffusion through endoplasmic reticulum supports elevated intraterminal Ca^{2+} levels needed to sustain synaptic release from rods in darkness. *J. Neurosci.* 35:11364–11373. https://doi.org/10.1523/JNEUROSCI.0754-15.2015

Chung, C., B. Barylko, J. Leitz, X. Liu, and E.T. Kavalali. 2010. Acute dynamin inhibition dissects synaptic vesicle recycling pathways that drive spontaneous and evoked neurotransmission. *J. Neurosci.* 30:1363–1376. https://doi.org/10.1523/JNEUROSCI.3427-09.2010

Cork, K.M., M.J. Van Hook, and W.B. Thoreson. 2016. Mechanisms, pools, and sites of spontaneous vesicle release at synapses of rod and cone photoreceptors. *Eur. J. Neurosci.* 44:2015–2027.

Courtney, N.A., H. Bao, J.S. Briguglio, and E.R. Chapman. 2019. Synaptotagmin 1 clamps synaptic vesicle fusion in mammalian neurons independent of complexin. *Nat. Commun.* 10:4076. https://doi.org/10.1038/s41467-019-12015-w

DeCoursey, T.E., and V.V. Cherny. 1998. Temperature dependence of voltage-gated H^+ currents in human neutrophils, rat alveolar epithelial cells, and mammalian phagocytes. *J. Gen. Physiol.* 112:503–522. https://doi.org/10.1085/jgp.112.4.503

Field, G.D., and F. Rieke. 2002. Nonlinear signal transfer from mouse rods to bipolar cells and implications for visual sensitivity. *Neuron.* 34:773–785. https://doi.org/10.1016/S0896-6273(02)00700-6

Gameiro, A., S. Braams, T. Rauen, and C. Grewer. 2011. The discovery of slowness: low-capacity transport and slow anion channel gating by the glutamate transporter EAAT5. *Biophys. J.* 100:2623–2632. https://doi.org/10.1016/j.bpj.2011.04.034

Grant, L., E. Yi, and E. Glowatzki. 2010. Two modes of release shape the postsynaptic response at the inner hair cell ribbon synapse. *J. Neurosci.* 30:4210–4220. https://doi.org/10.1523/JNEUROSCI.4439-09.2010

Grassmeyer, J.J., A.L. Cahill, C.L. Hays, C. Barta, R.M. Quadros, C.B. Gurumurthy, and W.B. Thoreson. 2019. Ca^{2+} sensor synaptotagmin-1 mediates exocytosis in mammalian photoreceptors. *eLife.* 8:e45946. https://doi.org/10.7554/eLife.45946

Grushin, K., J. Wang, J. Coleman, J.E. Rothman, C.V. Sindelar, and S.S. Krishnakumar. 2019. Structural basis for the clamping and Ca^{2+} activation of SNARE-mediated fusion by synaptotagmin. *Nat. Commun.* 10:2413. https://doi.org/10.1038/s41467-019-10391-x

Haeseleer, F., B. Williams, and A. Lee. 2016. Characterization of C-terminal splice variants of Cav1.4 Ca^{2+} channels in human retina. *J. Biol. Chem.* 291:15663–15673. https://doi.org/10.1074/jbc.M116.731737

Hasegawa, J., T. Obara, K. Tanaka, and M. Tachibana. 2006. High-density presynaptic transporters are required for glutamate removal from the first visual synapse. *Neuron.* 50:63–74. https://doi.org/10.1016/j.neuron.2006.02.022

Hays, C.L., J.J. Grassmeyer, X. Wen, R. Janz, R. Heidelberger, and W.B. Thoreson. 2020. Simultaneous release of multiple vesicles from rods involves synaptic ribbons and syntaxin 3B. *Biophys. J.* 118:967–979. https://doi.org/10.1016/j.bpj.2019.10.006

Heidelberger, R., M.M. Wang, and D.M. Sherry. 2003. Differential distribution of synaptotagmin immunoreactivity among synapses in the goldfish, salamander, and mouse retina. *Vis. Neurosci.* 20:37–49. https://doi.org/10.1017/S095252380320105X

Heidelberger, R., W.B. Thoreson, and P. Witkovsky. 2005. Synaptic transmission at retinal ribbon synapses. *Prog. Retin. Eye Res.* 24:682–720. https://doi.org/10.1016/j.preteyeres.2005.04.002

Herve, J.C., K. Yamaoka, V.W. Twist, T. Powell, J.C. Ellory, and L.C. Wang. 1992. Temperature dependence of electrophysiological properties of guinea pig and ground squirrel myocytes. *Am. J. Physiol.* 263:R177–R184.

Hille, B. 2001. Ion Channels of Excitable Membranes. Third edition. Sinauer, Sunderland, MA. xviii, 814 pp.

Hope, C.I., D.M. Sharp, A. Hemara-Wahanui, J.I. Sissingh, P. Lundon, E.A. Mitchell, M.A. Maw, and G.M. Clover. 2005. Clinical manifestations of a unique X-linked retinal disorder in a large New Zealand family with a novel mutation in *CACNA1F*, the gene responsible for CSNB2. *Clin. Exp. Ophthalmol.* 33:129–136. https://doi.org/10.1111/j.1442-9071.2005.00987.x

Kaeser, P.S., and W.G. Regehr. 2014. Molecular mechanisms for synchronous, asynchronous, and spontaneous neurotransmitter release. *Annu. Rev. Physiol.* 76:333–363. https://doi.org/10.1146/annurev-physiol-021113-170338

Kim, J.W., H.J. Yang, A.P. Oel, M.J. Brooks, L. Jia, D.C. Plachetzki, W. Li, W.T. Allison, and A. Swaroop. 2016. Recruitment of rod photoreceptors from short-wavelength-sensitive cones during the evolution of nocturnal vision in mammals. *Dev. Cell.* 37:520–532. https://doi.org/10.1016/j.devcel.2016.05.023

Koch, H.P., R.L. Brown, and H.P. Larsson. 2007. The glutamate-activated anion conductance in excitatory amino acid transporters is gated independently by the individual subunits. *J. Neurosci.* 27:2943–2947. https://doi.org/10.1523/JNEUROSCI.0118-07.2007

Koschak, A., D. Reimer, D. Walter, J.C. Hoda, T. Heinzle, M. Grabner, and J. Striessnig. 2003. Cav1.4alpha1 subunits can form slowly inactivating dihydropyridine-sensitive L-type Ca^{2+} channels lacking Ca^{2+}-dependent inactivation. *J. Neurosci.* 23:6041–6049. https://doi.org/10.1523/JNEUROSCI.23-14-06041.2003

Lee, S.C., and C. Deutsch. 1990. Temperature dependence of $K^{(+)}$-channel properties in human T lymphocytes. *Biophys. J.* 57:49–62. https://doi.org/10.1016/S0006-3495(90)82506-6

Linton, J.D., L.C. Holzhausen, N. Babai, H. Song, K.J. Miyagishima, G.W. Stearns, K. Lindsay, J. Wei, A.O. Chertov, T.A. Peters, et al. 2010. Flow of energy in the outer retina in darkness and in light. *Proc. Natl. Acad. Sci. USA.* 107:8599–8604. https://doi.org/10.1073/pnas.1002471107

Liu, H., H. Bai, E. Hui, L. Yang, C.S. Evans, Z. Wang, S.E. Kwon, and E.R. Chapman. 2014. Synaptotagmin 7 functions as a Ca^{2+}-sensor for synaptic vesicle replenishment. *eLife.* 3:e01524. https://doi.org/10.7554/eLife.01524

LoGiudice, L., and G. Matthews. 2009. The role of ribbons at sensory synapses. *Neuroscientist.* 15:380–391. https://doi.org/10.1177/1073858408331373

Luo, F., T. Bacaj, and T.C. Südhof. 2015. Synaptotagmin-7 is essential for Ca^{2+}-triggered delayed asynchronous release but not for Ca^{2+}-dependent vesicle priming in retinal ribbon synapses. *J. Neurosci.* 35:11024–11033. https://doi.org/10.1523/JNEUROSCI.0759-15.2015

Lv, C., T.J. Gould, J. Bewersdorf, and D. Zenisek. 2012. High-resolution optical imaging of zebrafish larval ribbon synapse protein RIBEYE, RIM2, and CaV 1.4 by stimulation emission depletion microscopy. *Microsc. Microanal.* 18:745–752. https://doi.org/10.1017/S1431927612000268

McKinney, R.A., M. Capogna, R. Dürr, B.H. Gähwiler, and S.M. Thompson. 1999. Miniature synaptic events maintain dendritic spines via AMPA receptor activation. *Nat. Neurosci.* 2:44–49. https://doi.org/10.1038/4548

McRory, J.E., J. Hamid, C.J. Doering, E. Garcia, R. Parker, K. Hamming, L. Chen, M. Hildebrand, A.M. Beedle, L. Feldcamp, et al. 2004. The *CACNA1F* gene encodes an L-type calcium channel with unique biophysical properties and tissue distribution. *J. Neurosci.* 24:1707–1718. https://doi.org/10.1523/JNEUROSCI.4846-03.2004

Mehta, B., J.B. Ke, L. Zhang, A.D. Baden, A.L. Markowitz, S. Nayak, K.L. Briggman, D. Zenisek, and J.H. Singer. 2014. Global Ca^{2+} signaling drives ribbon-independent synaptic transmission at rod bipolar cell synapses. *J. Neurosci.* 34:6233–6244. https://doi.org/10.1523/JNEUROSCI.5324-13.2014

Mennerick, S., and G. Matthews. 1996. Ultrafast exocytosis elicited by calcium current in synaptic terminals of retinal bipolar neurons. *Neuron.* 17:1241–1249. https://doi.org/10.1016/S0896-6273(00)80254-8

Mercer, A.J., M. Chen, and W.B. Thoreson. 2011. Lateral mobility of presynaptic L-type calcium channels at photoreceptor ribbon synapses. *J. Neurosci.* 31:4397–4406. https://doi.org/10.1523/JNEUROSCI.5921-10.2011

Morgans, C.W. 2001. Localization of the $\alpha_{(1F)}$ calcium channel subunit in the rat retina. *Invest. Ophthalmol. Vis. Sci.* 42:2414–2418.

Mostafavi, H., S. Thiyagarajan, B.S. Stratton, E. Karatekin, J.M. Warner, J.E. Rothman, and B. O'Shaughnessy. 2017. Entropic forces drive self-organization and membrane fusion by SNARE proteins. *Proc. Natl. Acad. Sci. USA.* 114:5455–5460. https://doi.org/10.1073/pnas.1611506114

Okawa, H., A.P. Sampath, S.B. Laughlin, and G.L. Fain. 2008. ATP consumption by mammalian rod photoreceptors in darkness and in light. *Curr. Biol.* 18:1917–1921. https://doi.org/10.1016/j.cub.2008.10.029

Otis, T.S., and C.E. Jahr. 1998. Anion currents and predicted glutamate flux through a neuronal glutamate transporter. *J. Neurosci.* 18:7099–7110. https://doi.org/10.1523/JNEUROSCI.18-18-07099.1998

Palmer, M.J., H. Taschenberger, C. Hull, L. Tremere, and H. von Gersdorff. 2003. Synaptic activation of presynaptic glutamate transporter currents

in nerve terminals. *J. Neurosci.* 23:4831–4841. https://doi.org/10.1523/JNEUROSCI.23-12-04831.2003

Pang, Z.P., T. Bacaj, X. Yang, P. Zhou, W. Xu, and T.C. Südhof. 2011. Doc2 supports spontaneous synaptic transmission by a $Ca^{(2+)}$-independent mechanism. *Neuron.* 70:244–251. https://doi.org/10.1016/j.neuron.2011.03.011

Pangrsic, T., J.H. Singer, and A. Koschak. 2018. Voltage-gated calcium channels: key players in sensory coding in the retina and the inner ear. *Physiol. Rev.* 98:2063–2096. https://doi.org/10.1152/physrev.00030.2017

Peloquin, J.B., C.J. Doering, R. Rehak, and J.E. McRory. 2008. Temperature dependence of Cav1.4 calcium channel gating. *Neuroscience.* 151:1066–1083. https://doi.org/10.1016/j.neuroscience.2007.11.053

Quadros, R.M., H. Miura, D.W. Harms, H. Akatsuka, T. Sato, T. Aida, R. Redder, G.P. Richardson, Y. Inagaki, D. Sakai, et al. 2017. Easi-CRISPR: a robust method for one-step generation of mice carrying conditional and insertion alleles using long ssDNA donors and CRISPR ribonucleoproteins. *Genome Biol.* 18:92. https://doi.org/10.1186/s13059-017-1220-4

Ramirez, D.M.O., D.C. Crawford, N.L. Chanaday, B. Trauterman, L.M. Monteggia, and E.T. Kavalali. 2017. Loss of Doc2-dependent spontaneous neurotransmission augments glutamatergic synaptic strength. *J. Neurosci.* 37:6224–6230. https://doi.org/10.1523/JNEUROSCI.0418-17.2017

Rao, R., G. Buchsbaum, and P. Sterling. 1994. Rate of quantal transmitter release at the mammalian rod synapse. *Biophys. J.* 67:57–63. https://doi.org/10.1016/S0006-3495(94)80454-0

Rao-Mirotznik, R., G. Buchsbaum, and P. Sterling. 1998. Transmitter concentration at a three-dimensional synapse. *J. Neurophysiol.* 80:3163–3172. https://doi.org/10.1152/jn.1998.80.6.3163

Rieke, F., and E.A. Schwartz. 1996. Asynchronous transmitter release: control of exocytosis and endocytosis at the salamander rod synapse. *J. Physiol.* 493:1–8. https://doi.org/10.1113/jphysiol.1996.sp021360

Sabatini, B.L., and W.G. Regehr. 1996. Timing of neurotransmission at fast synapses in the mammalian brain. *Nature.* 384:170–172. https://doi.org/10.1038/384170a0

Sampath, A.P., and F. Rieke. 2004. Selective transmission of single photon responses by saturation at the rod-to-rod bipolar synapse. *Neuron.* 41:431–443. https://doi.org/10.1016/S0896-6273(04)00005-4

Schein, S., and K.M. Ahmad. 2005. A clockwork hypothesis: synaptic release by rod photoreceptors must be regular. *Biophys. J.* 89:3931–3949. https://doi.org/10.1529/biophysj.105.070623

Schein, S., and K.M. Ahmad. 2006. Efficiency of synaptic transmission of single-photon events from rod photoreceptor to rod bipolar dendrite. *Biophys. J.* 91:3257–3267. https://doi.org/10.1529/biophysj.106.091744

Schmitz, F. 2009. The making of synaptic ribbons: how they are built and what they do. *Neuroscientist.* 15:611–624. https://doi.org/10.1177/1073858409340253

Schneeweis, D.M., and J.L. Schnapf. 1995. Photovoltage of rods and cones in the macaque retina. *Science.* 268:1053–1056. https://doi.org/10.1126/science.7754386

Schneider, N., S. Cordeiro, J.P. Machtens, S. Braams, T. Rauen, and C. Fahlke. 2014. Functional properties of the retinal glutamate transporters GLT-1c and EAAT5. *J. Biol. Chem.* 289:1815–1824. https://doi.org/10.1074/jbc.M113.517177

Sheng, Z., S.Y. Choi, A. Dharia, J. Li, P. Sterling, and R.H. Kramer. 2007. Synaptic Ca^{2+} in darkness is lower in rods than cones, causing slower tonic release of vesicles. *J. Neurosci.* 27:5033–5042. https://doi.org/10.1523/JNEUROSCI.5386-06.2007

Snellman, J., B. Mehta, N. Babai, T.M. Bartoletti, W. Akmentin, A. Francis, G. Matthews, W. Thoreson, and D. Zenisek. 2011. Acute destruction of the synaptic ribbon reveals a role for the ribbon in vesicle priming. *Nat. Neurosci.* 14:1135–1141. https://doi.org/10.1038/nn.2870

Specht, D., S.B. Wu, P. Turner, P. Dearden, F. Koentgen, U. Wolfrum, M. Maw, J.H. Brandstätter, and S. tom Dieck. 2009. Effects of presynaptic mutations on a postsynaptic Cacna1s calcium channel colocalized with mGluR6 at mouse photoreceptor ribbon synapses. *Invest. Ophthalmol. Vis. Sci.* 50:505–515. https://doi.org/10.1167/iovs.08-2758

Suryanarayanan, A., and M.M. Slaughter. 2006. Synaptic transmission mediated by internal calcium stores in rod photoreceptors. *J. Neurosci.* 26:1759–1766. https://doi.org/10.1523/JNEUROSCI.3895-05.2006

Szmajda, B.A., and S.H. Devries. 2011. Glutamate spillover between mammalian cone photoreceptors. *J. Neurosci.* 31:13431–13441. https://doi.org/10.1523/JNEUROSCI.2105-11.2011

Tan, G.M., D. Yu, J. Wang, and T.W. Soong. 2012. Alternative splicing at C terminus of Ca(V)1.4 calcium channel modulates calcium-dependent inactivation, activation potential, and current density. *J. Biol. Chem.* 287:832–847. https://doi.org/10.1074/jbc.M111.268722

Thoreson, W.B., and D.A. Burkhardt. 1991. Ionic influences on the prolonged depolarization of turtle cones in situ. *J. Neurophysiol.* 65:96–110. https://doi.org/10.1152/jn.1991.65.1.96

Thoreson, W.B., K. Rabl, E. Townes-Anderson, and R. Heidelberger. 2004. A highly Ca^{2+}-sensitive pool of vesicles contributes to linearity at the rod photoreceptor ribbon synapse. *Neuron.* 42:595–605. https://doi.org/10.1016/S0896-6273(04)00254-5

Thoreson, W.B., M.J. Van Hook, C. Parmelee, and C. Curto. 2016. Modeling and measurement of vesicle pools at the cone ribbon synapse: Changes in release probability are solely responsible for voltage-dependent changes in release. *Synapse.* 70:1–14. https://doi.org/10.1002/syn.21871

Torres-Salazar, D., and C. Fahlke. 2007. Neuronal glutamate transporters vary in substrate transport rate but not in unitary anion channel conductance. *J. Biol. Chem.* 282:34719–34726. https://doi.org/10.1074/jbc.M704118200

Tsukamoto, Y., and N. Omi. 2013. Functional allocation of synaptic contacts in microcircuits from rods via rod bipolar to AII amacrine cells in the mouse retina. *J. Comp. Neurol.* 521:3541–3555. https://doi.org/10.1002/cne.23370

Turecek, J., and W.G. Regehr. 2018. Synaptotagmin 7 mediates both facilitation and asynchronous release at granule cell synapses. *J. Neurosci.* 38:3240–3251. https://doi.org/10.1523/JNEUROSCI.3207-17.2018

Vaithianathan, T., D. Henry, W. Akmentin, and G. Matthews. 2016. Nanoscale dynamics of synaptic vesicle trafficking and fusion at the presynaptic active zone. *eLife.* 5:e13245. https://doi.org/10.7554/eLife.13245

Van Hook, M.J., and W.B. Thoreson. 2015. Weak endogenous Ca^{2+} buffering supports sustained synaptic transmission by distinct mechanisms in rod and cone photoreceptors in salamander retina. *Physiol. Rep.* 3:e12567. https://doi.org/10.14814/phy2.12567

Van Hook, M.J., C.M. Parmelee, M. Chen, K.M. Cork, C. Curto, and W.B. Thoreson. 2014. Calmodulin enhances ribbon replenishment and shapes filtering of synaptic transmission by cone photoreceptors. *J. Gen. Physiol.* 144:357–378. https://doi.org/10.1085/jgp.201411229

van Rossum, M.C., and R.G. Smith. 1998. Noise removal at the rod synapse of mammalian retina. *Vis. Neurosci.* 15:809–821. https://doi.org/10.1017/S0952523898155037

von Gersdorff, H., and G. Matthews. 1997. Depletion and replenishment of vesicle pools at a ribbon-type synaptic terminal. *J. Neurosci.* 17:1919–1927. https://doi.org/10.1523/JNEUROSCI.17-06-01919.1997

Waldner, D.M., N.T. Bech-Hansen, and W.K. Stell. 2018. Channeling vision: $Ca_V1.4$—a critical link in retinal signal transmission. *BioMed Res. Int.* 2018:7272630. https://doi.org/10.1155/2018/7272630

Wen, X., M.J. Van Hook, J.J. Grassmeyer, A.I. Wiesman, G.M. Rich, K.M. Cork, and W.B. Thoreson. 2018. Endocytosis sustains release at photoreceptor ribbon synapses by restoring fusion competence. *J. Gen. Physiol.* 150:591–611. https://doi.org/10.1085/jgp.201711919

Wu, S.M. 2010. Synaptic organization of the vertebrate retina: general principles and species-specific variations: the Friedenwald lecture. *Invest. Ophthalmol. Vis. Sci.* 51:1263–1274. https://doi.org/10.1167/iovs.09-4396

Xu, J., Z.P. Pang, O.H. Shin, and T.C. Südhof. 2009. Synaptotagmin-1 functions as a Ca^{2+} sensor for spontaneous release. *Nat. Neurosci.* 12:759–766. https://doi.org/10.1038/nn.2320

Yao, J., J.D. Gaffaney, S.E. Kwon, and E.R. Chapman. 2011. Doc2 is a Ca^{2+} sensor required for asynchronous neurotransmitter release. *Cell.* 147:666–677. https://doi.org/10.1016/j.cell.2011.09.046

Yuan, Y., H. Huo, and T. Fang. 2018. Effects of metabolic energy on synaptic transmission and dendritic integration in pyramidal neurons. *Front. Comput. Neurosci.* 12:79. https://doi.org/10.3389/fncom.2018.00079

Supplemental material

CICR was not required for coordinating bursts because they persisted after introducing dantrolene or a high concentration of ryanodine (100 µM; n = 4; Fig. S1) into rods through the patch pipette. Dantrolene did not extend interburst intervals (3,340 ± 2,489 ms; n = 6 rods, 2 animals) compared with control (2,756 ± 596 ms; n = 14 rods, 7 animals; P = 0.3, unpaired t test), nor did it reduce the number of quanta in each burst from control (dantrolene, 21 ± 9, n = 6; control, 17 ± 7, n = 22; P = 0.1, unpaired t test). The replenishment of internal stores by store-operated channels also does not appear necessary for bursts, because application of store-operated channel Orai/Stim1 blocker SKF96368 (10 µM) through the patch pipette did not eliminate bursting behavior (Fig. S1; n = 3 rods, 1 animal). We also tested whether feedback from horizontal cells to rods might be responsible for organizing bursts, but bursts at −40 mV appeared to be unchanged by bath application of 10 µM AMPA receptor blocker NBQX (Fig. S1; n = 3 rods, 1 animal). We only tested bursting with a single 30-s step to −40 mV with ryanodine, SKF96368, and NBQX, and this did not provide a large enough sample for quantifying specific burst parameters.

When rods were held at −30 or −40 mV for many seconds, we often observed large sustained inward currents that appeared to arise from $I_{Cl(Ca)}$ (Barnes and Deschênes, 1992; Thoreson and Burkhardt, 1991). These sustained currents were blocked by bath application of $CdCl_2$ (0.1 mM; Fig. S2) and were evoked more readily after lowering Ca^{2+} buffering to 0.1 mM EGTA, showing they were Ca^{2+} dependent. They were reduced in amplitude at more positive potentials and by replacing SCN with the less permeant anion gluconate (n = 5 rods, 3 animals) in the pipette solution, consistent with anion currents, but they were not blocked by TBOA (100 µM; n = 3 rods, n = 2 animals), indicating they were not glutamate transporter currents. These large Ca^{2+}-dependent currents could sometimes be observed even after strong buffering with 10 mM BAPTA, suggesting that buffers may become saturated by the continued influx of Ca^{2+} during 30-s steps.

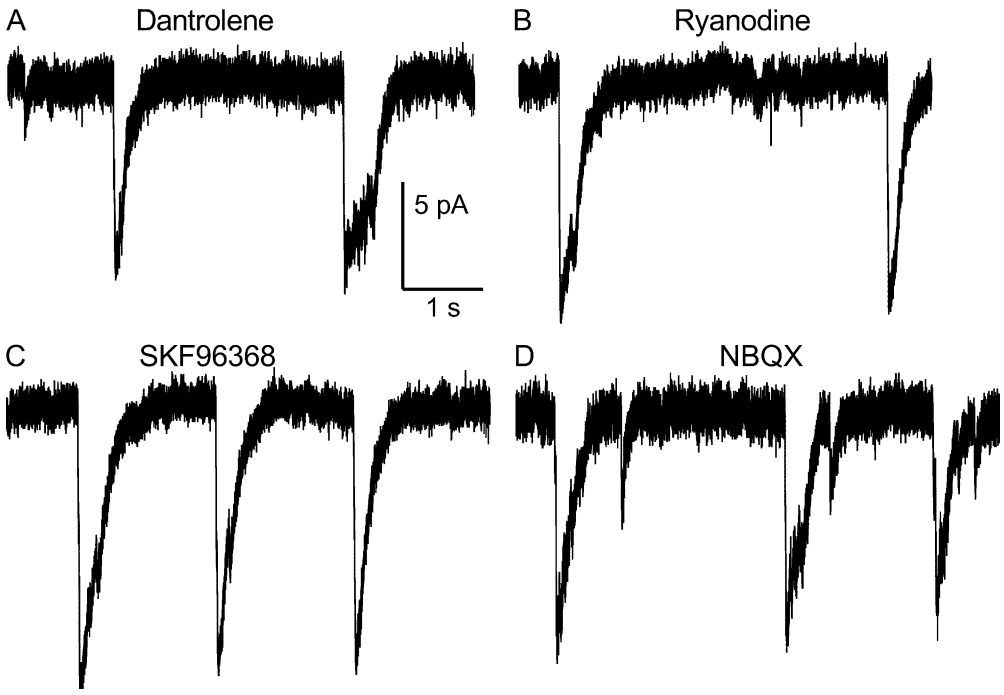

Figure S1. **CICR and horizontal feedback are not required for bursting in rods. (A and B)** Inhibiting CICR with a high concentration of dantrolene (100 µM) or ryanodine (100 µM) in the patch pipette did not eliminate bursting behavior. **(C)** Inhibiting the replenishment of internal Ca^{2+} stores with the store-operated calcium channel blocker SKF96368 (10 µM) in the bath also did not eliminate bursts. **(D)** Adding an AMPA receptor blocker, NBQX (10 µM), to the bath to block horizontal cell feedback did not eliminate bursting.

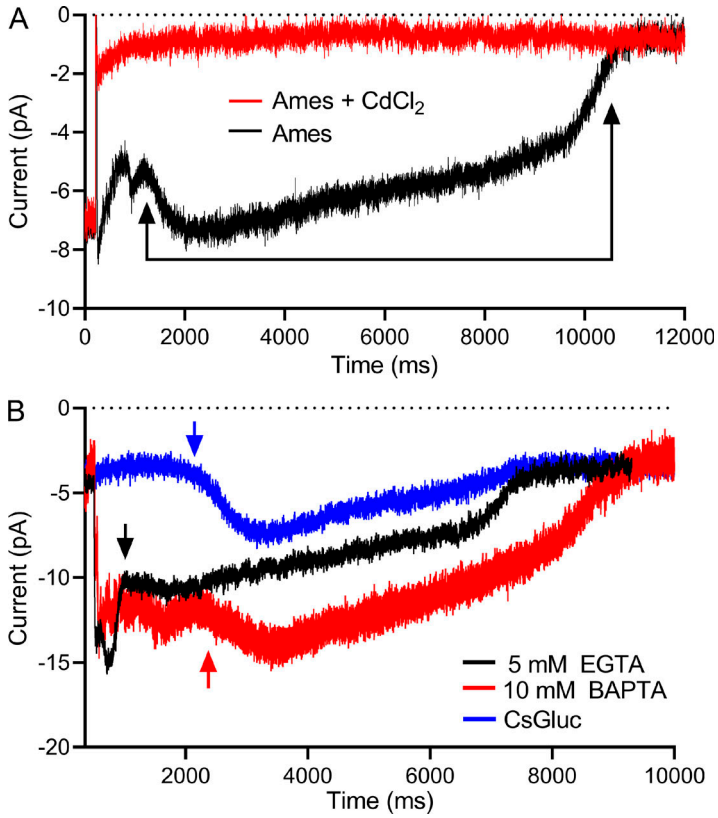

Figure S2. **Prolonged Ca^{2+}-activated Cl^- currents ($I_{Cl(Ca)}$) emerge during sustained depolarization. (A)** Representative current trace with 5 mM EGTA buffering (black trace) shows that these large inward currents (denoted by the brackets) were eliminated when $CdCl_2$ (red trace) was included in the Ames extracellular solution. **(B)** Using a Cs-gluconate (CsGluc)–based internal solution (blue trace) rather than the KSCN solution (black trace) reduced $I_{Cl(Ca)}$. $I_{Cl(Ca)}$ persisted even with 10 mM BAPTA (red trace) in the KSCN internal solution, suggesting that Ca^{2+} buffers could be saturated by the sustained Ca^{2+} influx during 30-s depolarizing steps. Arrows show the start times for $I_{Cl(Ca)}$ events.